Compression Strength of Composite Primary Structural Components

Semiannual Status Report

Eric R. Johnson
Principal Investigator

Performance Period: May 1, 1994 to October 31, 1994

NASA Grant NAG-1-537

Aerospace and Ocean Engineering Department
Virginia Polytechnic Institute and State University
Blacksburg, Virginia 24061-0203

December, 1994

Technical Monitor: Dr. James H. Starnes, Jr., Head
Structural Mechanics Branch
National Aeronautics and Space Administration
Langley Research Center
Hampton, Virginia 23681-0001

INTRODUCTION

Research continued on *Pressure Pillowing of an Orthogonally Stiffened Cylindrical Shell.* The motivation for this project is the planned utilization of advanced composite materials in the fuselage for large transport aircraft. In particular, the focus of this activity is the effect of cabin pressurization on the stiffener-to-skin joint. The design of stiffener-to-skin joints is one of the major technology issues in utilizing graphite/epoxy composites in the fuselage of a large transport aircraft. The manner in which the loads are transferred in the stiffener-to-skin joints under internal pressurization is important for determining the load capacity of these joints.

The objective of this project is to develop analyses of an orthogonally stiffened composite cylindrical shell subjected to internal pressure. These analyses are used to study the distribution of the interacting loads between the shell and stiffeners, and to study the pillowing of the shell, for a geometry and pressure typical of a large transport aircraft. Primarily the aim is to understand the fundamental mechanics of the load transfer in the vicinity of the shell-ring-stringer joint. Secondly, these analyses can be used in parametric studies of joint response, and perhaps for design. A potential benefit of such an analysis/design capability is to use fewer expensive fasteners in the graphite/epoxy fuselage. Where fasteners are required in a graphite/epoxy structure, aluminium fasteners cannot be used because of galvanic corrosion to the metal. More expensive fasteners, like titanium, are required to avoid corrosion.

RESEARCH ACCOMPLISHED

A conference paper was presented, and an extended abstract of it appears in the conference proceedings. The citation for the abstract and presentation are given below.

- Johnson, E.R., and Rastogi, N., "Influence of an Asymmetric Ring on the Modeling of an Orthogonally Stiffened Cylindrical Shell," Proceedings of International Conference on **Composites Engineering** ICCE/1, David Hui, Editor, International Community for Composites Engineering, August 1994, pp. 237 & 238.

- Johnson, E.R. (speaker), and Rastogi, N., "Influence of an Asymmetric Ring on the Modeling of an Orthogonally Stiffened Cylindrical Shell," *International Conference on Composites Engineering*, Sheraton Hotel Downtown, New Orleans, Louisiana, August 28 - 31, 1994, Session 13f: Composite Structures 1.

Work continued on the effect of a ring, or frame, with an asymmetrical open cross section on the response. Since the ring has an asymmetrical section, it twists and bends out-of-plane under the internal pressure load in addition to bending in its plane and stretching along its circumference. For the structural repeating unit shown in the Figure below, the asymmetrical section ring results in loss of symmetry of the deformation about the θ-axis. (Symmetry about the x-axis is preserved since the stringer cross section is assumed to be symmetric.)

The major new feature incorporated into the analysis was the warping deformation of the ring's cross section due to torsion. This warping deformation is in addition to a previous extension of the model to include deformations due to transverse shear in the stiffeners and in the shell.

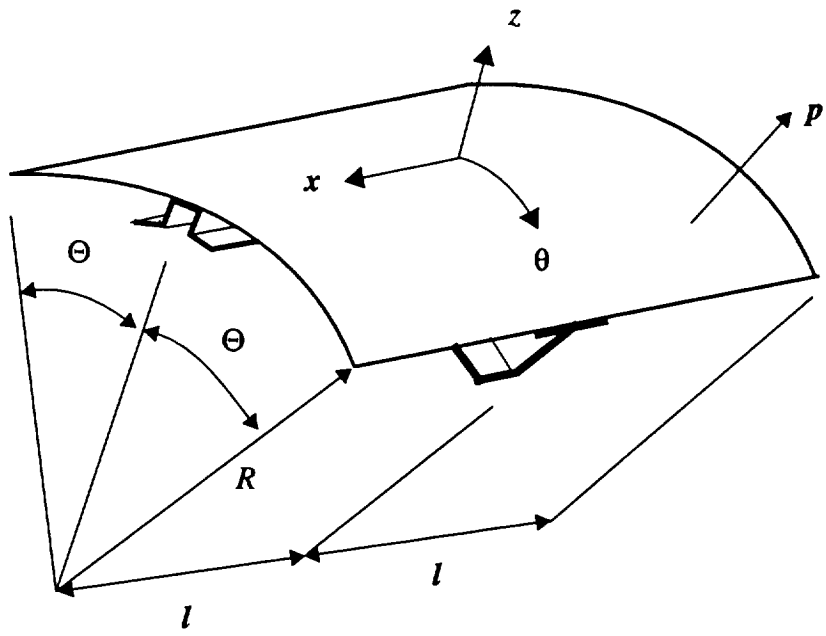

Figure: Structural repeating unit of an orthogonally stiffened cylindrical shell subjected to a internal pressure *p*.

Inclusion of warping was found to significantly change the torsion and out-of-plane bending response of the ring, and to change the distributions and magnitudes of the interacting line loads between the stiffeners and the shell. For example, the direction of the rotation about the circumferential axis of each of the structural elements at the shell-ring-stringer joint was change by the inclusion of this warping deformation. Also, the circumferential component of the moment resultant at the joint due to these interacting load intensities was increased by the inclusion of warping deformation. These results are detailed in the Appendix of this report.

APPENDIX

Analysis of an Internally Pressurized Orthogonally Stiffened Cylindrical Shell with an Asymmetrical Section Ring

ANALYSIS OF AN INTERNALLY PRESSURIZED ORTHOGONALLY STIFFENED CYLINDRICAL SHELL WITH AN ASYMMETRICAL SECTION RING

Naveen Rastogi* and Eric R. Johnson†

Virginia Polytechnic Institute and State University

Blacksburg, Virginia 24061

ABSTRACT

The linear elastic response is determined for an internally pressurized, long circular cylindrical shell stiffened on the inside by a regular arrangement of identical stringers and identical rings. Periodicity of this configuration permits the analysis of a portion of the shell wall centered over a generic stringer-ring joint; i.e., a unit cell model. The stiffeners are modeled as discrete beams, and the stringer is assumed to have a symmetrical cross section and the ring an asymmetrical section. Asymmetry causes out-of-plane bending and torsion of the ring. Displacements are assumed as truncated double Fourier series plus simple terms in the axial coordinate to account for the closed end pressure vessel effect (a non-periodic effect). The interacting line loads between the stiffeners and the inside shell wall are Lagrange multipliers in the formulation, and they are also assumed as truncated Fourier series. Displacement continuity constraints between the stiffeners and shell along the contact lines are satisfied point-wise. Equilibrium is imposed by the principle of virtual work. A composite material crown panel from the fuselage of a large transport aircraft is the numerical example. The distributions of the interacting line loads, and the out-of-plane bending moment and torque in the ring, are strongly dependent on modeling the deformations due to transverse shear and cross-sectional warping of the ring in torsion.

---

* Graduate Research Assistant, Aerospace and Ocean Engineering

† Professor of Aerospace and Ocean Engineering

INTRODUCTION

The design of stiffener-to-skin joints is one of the major technology issues in utilizing graphite-epoxy composites in the fuselage of a large transport aircraft (Jackson, et al., 1984). Stiffeners can be attached to the skin by either fasteners, co-curing, adhesive bonding, or some combination of these methods. Where fasteners are required in a graphite-epoxy structure, aluminium fasteners cannot be used because of galvanic corrosion to the metal. More expensive fasteners, like titanium, are required to avoid corrosion. Hence to reduce manufacturing costs, mechanical fasteners can be eliminated in favor of bonded joints. As an example, a graphite-epoxy crown panel for the fuselage of a large transport aircraft was recently fabricated without fasteners by co-curing the stringers and co-bonding the rings, or frames, to the skin (Ilcewicz, et al., 1992; Swanson, et al., 1992). Also, the curved graphite-epoxy fuselage frames were manufactured by resin transfer molding into two-dimensional braided preforms of net structural shape (Jackson, 1994). Clearly, the strength of the bond line is a critical issue for these primary fuselage structures made from advanced composite materials. The purpose of this paper is to analyze the load transfer in bonded stiffener-to-skin joints under cabin pressurization. Internal pressure is an important load to consider because it tends to cause peel stresses in the bond line which are particularly debilitating in adhesive joints.

An idealized structural model of the fuselage is analyzed. This configuration is a long circular cylindrical shell stiffened on the inside by a regular arrangement of identical stringers and identical rings (frames). Periodicity of this configuration permits the analysis of a portion of the shell wall centered over a generic stringer-ring joint; i.e., deformation of a structural unit cell determines the deformation of the entire shell. The stringer is assumed to have a symmetrical cross section , and the frame is assumed to have an asymmetrical open section. Asymmetrical open section frames are commonly used as transverse stiffeners in the fuselage structure. The stiffeners are modeled as discrete beams perfectly bonded to the inside shell wall, so that the interacting loads between the stiffeners and shell wall are line

load intensities. These line load intensities represent resultants of the tractions integrated across the width of the attachment flanges of the stiffeners.

Mathematical formulations for the linear elastic response presented in this paper include the effect of transverse shear deformations and the effect of warping of the ring's cross section due to torsion. These effects are important when the ring has an asymmetrical cross section, because the loss of symmetry in the problem results in torsion of the ring, as well as out-of-plane bending, and a concomitant rotation of the joint at the stiffener intersection about the circumferential axis. This stringer-ring-shell joint is modeled in an idealized manner; the stiffeners are mathematically permitted to pass through one another without contact, but do interact indirectly through their mutual contact with the shell at the joint. Restraint of cross-sectional warping, as occurs here in the ring due to contact with the shell, is an important contributor to the normal stresses in thin-walled open section bars, as was demonstrated by Hoff (1945). Based on transverse shear deformation and cross-sectional warping of the ring, four structural models can be defined. The simplest model uses non-transverse-shear-deformable theory, or classical theory, and neglects warping due to torsion. The most complex model includes both effects. Intermediate complexity models occurs for inclusion of one effect without the other.

For symmetric section stiffeners, the response of the unit cell is symmetric about the stringer axis and the ring axis, and there is no rotation of stringer-ring-shell joint. Results have been published for the linear response (Wang and Hsu, 1985) and for the geometrically nonlinear response (Johnson and Rastogi, 1994) of a symmetric configuration subjected to internal pressure.

MATHEMATICAL MODEL

An idealized mathematical model is assumed for the semi-monocoque fuselage to study the generic characteristics of the response in the vicinity of the stiffeners' intersection. The model is of a very long circular cylindrical shell internally stiffened by identical stringers equally spaced around the circumference, and identical frames

or rings, equally spaced along the length. In general, the spacing of the stringers is not the same as that of the rings. The structure is periodic both longitudinally and circumferentially, and the loading is spatially uniform. Consequently, a structural repeating unit (or unit cell) can be defined whose deformation determines the deformation of the entire structure. A typical repeating unit consists of a portion of the shell wall centered over portions of stringer and ring as shown in Fig. 1. The radius of the middle surface of the undeformed cylindrical shell is denoted by R, and the thickness of the shell is denoted by t. Axial coordinate x and the circumferential angle θ are lines of curvature on the middle surface, and the thickness coordinate is denoted by z, with $-t/2 \leq z \leq t/2$. The origin of the surface coordinates is centered over the stiffeners intersection so that $-l \leq x \leq l$ and $-\Theta \leq \theta \leq \Theta$, where $2l$ is the axial length, and $2R\Theta$ is the circumferential arc length of the repeating unit.

The stiffeners are mathematically modeled as one-dimensional elements, or discrete beams, so that the actions transmitted by the stiffeners to the inside of the shell wall are represented by distributed line load intensities. In this paper it is assumed that the stringer is symmetric about the x-z plane through its centroidal axis and the ring is asymmetric. On the basis of the symmetry about the x-axis for the unit, only the interacting line load components tangent and normal to the stringer are included in the analyses. The shell-stringer interacting force components per unit length along the contact lines are denoted by $\lambda_{xs}(x)$ for the component tangent to the stringer, and $\lambda_{zs}(x)$ for the component normal to the stringer. However, due to an asymmetrical cross section ring, the components of line loads between shell and the ring consist of three force intensities and two moment intensities. The three shell-ring interacting force components per unit length along the contact lines are denoted by $\lambda_{xr}(\theta)$ for the component acting in the axial direction, $\lambda_{\theta r}(\theta)$ for the component tangent to the ring, and $\lambda_{zr}(\theta)$ for the component normal to the ring. The two shell-ring interacting moment components per unit length along the contact lines are denoted by $\Lambda_{\theta r}(\theta)$ for the component tangent to the ring and $\Lambda_{zr}(\theta)$

for the component normal to the ring. These interacting loads acting in a positive sense on the inside surface of the shell are shown in Fig. 2. The purpose of the analysis is to determine these distributed line load intensities and also, to examine the differences in their magnitudes and distributions for the four structural models described earlier.

For all the structural models, the linear elastic response of the repeating unit to internal pressure is obtained by utilizing Ritz method and the principle of virtual work applied separately to the shell, stringer, and ring. The virtual work functionals are augmented by Lagrange multipliers to enforce kinematic constraints between the structural components of the repeating unit. The Lagrange multipliers represent the interacting line loads between the stiffeners and the shell. Displacements are separately assumed for the shell, stringer, and the ring.

TRANSVERSE SHEAR DEFORMATION FORMULATIONS

Shell

A consistent first order transverse shear deformation theory is developed to model the shell. Based on the assumption that the shell thickness t is relatively small and hence, does not change during loading, the displacements at an arbitrary material point in the shell are approximated by

$$U(x,\theta,z) = u(x,\theta) + z\phi_x(x,\theta) \tag{1}$$

$$V(x,\theta,z) = v(x,\theta) + z\phi_\theta(x,\theta) \tag{2}$$

$$W(x,\theta,z) = w(x,\theta) \tag{3}$$

where $u(x,\theta)$, $v(x,\theta)$ and $w(x,\theta)$ are the displacements of the points of the reference surface, and $\phi_x(x,\theta)$ and $\phi_\theta(x,\theta)$ are the rotations of the normal to the reference surface as shown in Fig. 3(a). Using Eqs. (1) to (3) and assuming small displacement gradients, the three-dimensional engineering strains are

$$e_{xx} = \epsilon_{xx} + z\kappa_{xx} \qquad e_{\theta\theta} = \frac{\epsilon_{\theta\theta} + z\kappa_{\theta\theta}}{(1+\frac{z}{R})} \qquad e_{zz} = 0 \tag{4}$$

$$e_{x\theta} = \frac{\gamma_{x\theta} + z(1+\frac{z}{2R})\bar{\kappa}_{x\theta} + \frac{z^2}{2R}\tilde{\kappa}_{x\theta}}{(1+\frac{z}{R})} \tag{5}$$

$$e_{xz} = \gamma_{xz} \qquad e_{\theta z} = \frac{\gamma_{\theta z}}{(1+\frac{z}{R})} \tag{6}$$

The transverse shear strains e_{xz} and $e_{\theta z}$ represent average transverse shearing strains through the thickness of the shell since these strains contain derivatives of the displacements in z, and Eqs. (1) to (3) are approximate in the z-coordinate. In Eqs. (4) to (6), the two-dimensional, or shell, strain measures, which are independent of the z-coordinate, are defined by

$$\epsilon_{xx} = \frac{\partial u}{\partial x} \qquad \kappa_{xx} = \frac{\partial \phi_x}{\partial x} \tag{7}$$

$$\epsilon_{\theta\theta} = \frac{1}{R}\frac{\partial v}{\partial \theta} + \frac{w}{R} \qquad \kappa_{\theta\theta} = \frac{1}{R}\frac{\partial \phi_\theta}{\partial \theta} \tag{8}$$

$$\gamma_{x\theta} = \frac{\partial v}{\partial x} + \frac{1}{R}\frac{\partial u}{\partial \theta} \tag{9}$$

$$\bar{\kappa}_{x\theta} = \frac{\partial \phi_\theta}{\partial x} + \frac{1}{R}\frac{\partial \phi_x}{\partial \theta} + \frac{1}{R}\frac{\partial v}{\partial x} \tag{10}$$

$$\tilde{\kappa}_{x\theta} = \frac{\partial \phi_\theta}{\partial x} - \frac{1}{R}\frac{\partial \phi_x}{\partial \theta} - \frac{1}{R}\frac{\partial v}{\partial x} \tag{11}$$

$$\gamma_{xz} = \phi_x + \frac{\partial w}{\partial x} \qquad \gamma_{\theta z} = \phi_\theta - \frac{v}{R} + \frac{1}{R}\frac{\partial w}{\partial \theta} \tag{12}$$

If we set the (average) transverse shear strains in Eq. (6) to zero, then the rotations of the normal are

$$\phi_x = -\frac{\partial w}{\partial x} \tag{13}$$

$$\phi_\theta = \frac{v}{R} - \frac{1}{R}\frac{\partial w}{\partial \theta} \tag{14}$$

so that

$$\kappa_{x\theta} = \bar{\kappa}_{x\theta} = -\frac{2}{R}\frac{\partial^2 w}{\partial x \partial \theta} + \frac{2}{R}\frac{\partial v}{\partial x} \qquad \tilde{\kappa}_{x\theta} = 0 \tag{15}$$

Hence, the thickness distribution of the shear strain reduces to

$$e_{x\theta} = \frac{\gamma_{x\theta} + z(1+\frac{z}{2R})\kappa_{x\theta}}{(1+\frac{z}{R})} \tag{16}$$

which coincides with the results of Novozhilov's (1964) classical shell theory.

It is evident from Eq. (5) that three shell strain measures are needed to represent the shear strain distribution through the thickness in the transverse shear deformation shell theory. Whereas, only two shell strain measures are required in classical shell theory to represent the shearing strain distribution through the thickness (refer to Eq. (16)). Also it can be shown that under rigid body rotation of the shell, the nine shell strain measures, given by Eqs. (7) through (12) vanish. (For Novozhilov's classical shell theory, six shell strain measures given by Eqs. (7-9) and (15) vanish under rigid body rotations).

The physical stress resultants and stress couples for the shell in terms of stress components are given, in the usual way, by

$$\begin{aligned}
(N_{xx},\ M_{xx}) &= \int_t (1, z)\sigma_{xx}(1 + \frac{z}{R})\ dz \\
(N_{\theta\theta},\ M_{\theta\theta}) &= \int_t (1, z)\sigma_{\theta\theta}\ dz \\
(N_{x\theta},\ M_{x\theta}) &= \int_t (1, z)\sigma_{x\theta}(1 + \frac{z}{R})\ dz \\
(N_{\theta x},\ M_{\theta x}) &= \int_t (1, z)\sigma_{\theta x}\ dz \\
Q_x &= \int_t \sigma_{xz}(1 + \frac{z}{R})\ dz \\
Q_\theta &= \int_t \sigma_{\theta z} dz
\end{aligned} \tag{17}$$

A generalized 9×1 stress vector for the shell is defined by

$$\vec{\sigma}_{shell} = [N_{xx}, N_{\theta\theta}, N_{\theta x}, M_{xx}, M_{\theta\theta}, \bar{M}_{x\theta}, \tilde{M}_{x\theta}, Q_x, Q_\theta]^T \tag{18}$$

in which $\bar{M}_{x\theta}$ and $\tilde{M}_{x\theta}$ are the mathematical quantities conjugate to the modified twisting measures $\bar{\kappa}_{x\theta}$ and $\tilde{\kappa}_{x\theta}$, respectively, and are defined in terms of the physical stress couples by

$$\bar{M}_{x\theta} = \frac{1}{2}(M_{x\theta} + M_{\theta x}) \qquad \tilde{M}_{x\theta} = \frac{1}{2}(M_{x\theta} - M_{\theta x}) \tag{19}$$

The nine elements of the stress vector in Eq. (18) and the relations of Eq. (19) determine all the stress resultants and stress couples listed in Eq. (17) except for shear resultant $N_{x\theta}$. The shear stress resultant $N_{x\theta}$ is determined from moment equilibrium about the normal for an element of the shell. This so-called sixth equilibrium equation is

$$N_{x\theta} = N_{\theta x} + \frac{M_{\theta x}}{R} \tag{20}$$

The generalized strain vector for the shell is

$$\vec{\epsilon}_{shell} = [\epsilon_{xx}, \epsilon_{\theta\theta}, \gamma_{x\theta}, \kappa_{xx}, \kappa_{\theta\theta}, \bar{\kappa}_{x\theta}, \tilde{\kappa}_{x\theta}, \gamma_{xz}, \gamma_{\theta z}]^T \tag{21}$$

This strain vector is conjugate to the stress vector in the sense that the internal virtual work for the shell is given by

$$\delta \mathcal{W}^{int}_{shell} = \iint_S \delta \vec{\epsilon}^T_{shell}\ \vec{\sigma}_{shell}\ dS \tag{22}$$

where S denotes the area of the reference surface and $dS = dxRd\theta$. This expression for the internal virtual work can be derived from three-dimensional elasticity theory by using Eqs. (4) to (6) for the thickness distributions of the strains and the definitions of the resultants given by Eqs. (17) and (19).

Consistent with the transverse shear deformation theory, the linear elastic constitutive law for a laminated composite shell wall is given by

$$\begin{Bmatrix} N_{xx} \\ N_{\theta\theta} \\ N_{\theta x} \\ M_{xx} \\ M_{\theta\theta} \\ \bar{M}_{x\theta} \\ \tilde{M}_{x\theta} \end{Bmatrix} = \begin{bmatrix} A_{11} & A_{12} & A_{16} & B_{11} & B_{12} & B^1_{16} & B^2_{16} \\ A_{12} & A_{22} & A_{26} & B_{12} & B_{22} & B^1_{26} & B^2_{26} \\ A_{16} & A_{26} & A_{66} & B_{61} & B_{62} & B^1_{66} & B^2_{66} \\ B_{11} & B_{12} & B_{61} & D_{11} & D_{12} & D^1_{16} & D^2_{16} \\ B_{12} & B_{22} & B_{62} & D_{12} & D_{22} & D^1_{26} & D^2_{26} \\ B^1_{16} & B^1_{26} & B^1_{66} & D^1_{16} & D^1_{26} & D^{11}_{66} & D^{12}_{66} \\ B^2_{16} & B^2_{26} & B^2_{66} & D^2_{16} & D^2_{26} & D^{12}_{66} & D^{22}_{66} \end{bmatrix} \begin{Bmatrix} \epsilon_{xx} \\ \epsilon_{\theta\theta} \\ \gamma_{x\theta} \\ \kappa_{xx} \\ \kappa_{\theta\theta} \\ \bar{\kappa}_{x\theta} \\ \tilde{\kappa}_{x\theta} \end{Bmatrix} \tag{23}$$

and

$$\begin{Bmatrix} Q_x \\ Q_\theta \end{Bmatrix} = \begin{bmatrix} A_{44} & A_{45} \\ A_{45} & A_{55} \end{bmatrix} \begin{Bmatrix} \gamma_{xz} \\ \gamma_{\theta z} \end{Bmatrix} \tag{24}$$

in which stiffnesses A_{ij}, B_{ij} and D_{ij} are given in Appendix. The transverse shear stiffnesses, A_{44}, A_{45}, and A_{55} can be calculated by two different methods. The first method is based on the assumption of constant transverse shear strain distribution through the thickness, and the second method is based on the assumption of constant transverse şhear stress distribution through the thickness. In the present analysis, we have used the first method to compute the transverse shear stiffnesses.

The statement of virtual work is

$$\delta \mathcal{W}^{int}_{shell} = \delta \mathcal{W}^{ext}_{p} + \delta \mathcal{W}^{ext}_{\lambda} \tag{25}$$

where the external virtual work for a cylindrical shell under constant internal pressure, including an axial load due to the closed-end effect, is written as

$$\delta \mathcal{W}^{ext}_{p} = \iint_{S} p\ \delta w\ dS \quad + \quad p \int_{-\Theta}^{\Theta} \frac{R^2}{2} d\theta\ [\delta u(l,\theta) - \delta u(-l,\theta)] \tag{26}$$

and the external (or augmented) virtual work due to the interacting loads is

$$\begin{aligned}
\delta \mathcal{W}^{ext}_{\lambda} = & \int_{-l}^{l} \Big\{ \lambda_{xs}(x)\big[\delta u(x,0) - \frac{t}{2}\delta\phi_x(x,0)\big] + \lambda_{zs}(x)\delta w(x,0) \Big\}\ dx \\
& + \int_{-\Theta}^{\Theta} \Big\{ \lambda_{xr}(\theta)\big[\delta u(0,\theta) - \frac{t}{2}\delta\phi_x(0,\theta)\big] + \lambda_{\theta r}(\theta)\big[\delta v(0,\theta) - \frac{t}{2}\delta\phi_\theta(0,\theta)\big] \\
& + \lambda_{zr}(\theta)\delta w(0,\theta) - \Lambda_{\theta r}(\theta)\delta(\frac{\partial w}{\partial x}|_{x=0}) + \Lambda_{zr}(\theta)\delta(\frac{\partial v}{\partial x}|_{x=0} \\
& - \frac{t}{2}\frac{\partial \phi_\theta}{\partial x}|_{x=0}) \Big\}\ (R - \frac{t}{2}) d\theta - Q[\delta u(l,0) - \delta u(-l,0)]
\end{aligned} \tag{27}$$

The axial force Q in Eq. (27) is an additional Lagrange multiplier that accounts for axial load sharing between the stringer and shell.

Stringer

Stringer displacements $u_s(x)$ and $w_s(x)$, and the rotation of the normal $\phi_{\theta s}(x)$ are shown in Fig. 3(b). Based on transverse shear deformation theory, the virtual work expression for the stringer is

$$\int_{-l}^{l} [N_{xs}\delta\epsilon_{xs} + M_{\theta s}\delta\kappa_{\theta s} + V_{zs}\delta\gamma_{zs}]dx = -\int_{-l}^{l} \Big\{\lambda_{xs}(x)[\delta u_s(x) + e_s\delta\phi_{\theta s}(x)] + \lambda_{zs}(x)\delta w_s(x)\Big\}\, dx + Q[\delta u_s(l) - \delta u_s(-l)] \tag{28}$$

in which N_{xs} is the axial force in the stringer, $M_{\theta s}$ is the bending moment, V_{zs} is the transverse shear force, ϵ_{xs} is the normal strain of the centroidal line, the product $z\kappa_{\theta s}$ is the portion of the axial normal strain due to bending, γ_{zs} is the transverse shear strain, and e_s is the radial distance from the stringer centroid to the contact line along the shell inside surface. The strain-displacement relations and Hooke's law for the stringer are

$$\epsilon_{xs} = u'_s \qquad \kappa_{\theta s} = \phi'_{\theta s} \qquad \gamma_{zs} = \phi_{\theta s} + w'_s \tag{29}$$

$$N_{xs} = (EA)_s\epsilon_{xs} \qquad M_{\theta s} = (EI)_s\kappa_{\theta s} \qquad V_{zs} = (GA)_s\gamma_{zs} \tag{30}$$

in which the prime denotes an ordinary derivative with respect to x.

Ring

Ring displacements are denoted $u_r(\theta)$, $v_r(\theta)$, and $w_r(\theta)$, and the rotations are denoted by $\phi_{xr}(\theta)$, $\phi_{\theta r}(\theta)$, and $\phi_{zr}(\theta)$ as shown in Fig. 3(c). The structural model is based on transverse shear deformation theory and includes cross-sectional warping due to torsion. The extension of classical thin-walled, open section curved bar theory to laminated composite materials was developed by Woodson, Johnson, and Haftka (1993). However, Woodson et al. (1993) did not consider transverse shear deformations.

The statement of virtual work is

$$\int_{-\Theta}^{\Theta} [N_{\theta r}\delta\epsilon_{\theta r} + M_{xr}\delta\kappa_{xr} + M_{zr}\delta\kappa_{zr} + T_{sr}\delta\tau_r + M_{\omega r}\delta(\dot{\tau}_r/R_0) + V_{xr}\delta\gamma_{xr} + V_{zr}\delta\gamma_{zr}]*$$

$$R_0 d\theta = -\int_{-\Theta}^{\Theta} \Big\{ \lambda_{xr}(\theta)\big[\delta u_r(\theta) + e_r\delta\phi_{\theta r}(\theta)\big] + \lambda_{\theta r}(\theta)\big[\delta v_r(\theta) + e_r\delta\phi_{xr}(\theta) - \omega_0\delta\tau_r(\theta)\big]$$

$$+ \lambda_{zr}(\theta)\delta w_r(\theta) + \Lambda_{\theta r}(\theta)\delta\phi_{\theta r}(\theta) + \Lambda_{zr}(\theta)\big[\delta\phi_{zr}(\theta) - \omega_1\delta\tau_r(\theta)\big] \Big\} \left(1 + \frac{e_r}{R_0}\right) R_0 \; d\theta \tag{31}$$

in which $N_{\theta r}$ is the circumferential force, M_{xr} is the in-plane bending moment, M_{zr} is the out-of-plane bending moment, $M_{\omega r}$ is the circumferential bimoment, T_{sr} is the St. Venant torque, V_{xr} is transverse shear force in the x-direction, V_{zr} is transverse shear force in the z-direction, $\epsilon_{\theta r}$ is the circumferential normal strain of the centroidal arc, κ_{xr} is the in-plane bending rotation gradient, κ_{zr} is the out-of-plane bending rotation gradient, τ_r is the twist rate, γ_{xr} is transverse shear strain in θ-z plane, γ_{zr} is transverse shear strain in x-z plane, e_r is the distance from the ring reference arc to the contact line along the shell inside surface, and R_0 is the radius of ring reference arc. Parameters ω_0 and ω_1 are the constant coefficients in the contour warping function, $\omega(x) = \omega_0 + x\omega_1$, for the attachment flange of the ring. The rotations and strain-displacement relations are

$$\begin{aligned} &\epsilon_{\theta r} = \frac{1}{R_0}(\dot{v}_r + w_r) \qquad && \kappa_{xr} = \frac{1}{R_0}\dot{\phi}_{xr} \qquad && \kappa_{zr} = \frac{1}{R_0}(\dot{\phi}_{zr} - \phi_{\theta r}) \\ &\tau_r = \frac{1}{R_0}(\dot{\phi}_{\theta r} + \phi_{zr}) \qquad && \gamma_{zr} = \phi_{xr} - \frac{1}{R_0}(v_r - \dot{w}_r) \qquad && \gamma_{xr} = \phi_{zr} + \frac{1}{R_0}\dot{u}_r \end{aligned} \tag{32}$$

in which ϕ_{xr} is the rotation around x-axis, $\phi_{\theta r}$ is the rotation around θ-axis, ϕ_{zr} is the rotation around z-axis, and the over-dot denotes an ordinary derivative with respect to θ. It is assumed that the shear forces are decoupled from extension, bending, and torsional deformations of the ring. Thus, the material law for the ring

is

$$\begin{Bmatrix} N_{\theta r} \\ M_{xr} \\ M_{zr} \\ M_{\omega r} \\ T_{sr} \\ V_{xr} \\ V_{zr} \end{Bmatrix} = \begin{bmatrix} EA & ES_x & -ES_z & -ES_\omega & EH & 0 & 0 \\ ES_x & EI_{xx} & -EI_{zx} & -EI_{\omega x} & EH_c & 0 & 0 \\ -ES_z & -EI_{zx} & EI_{zz} & EI_{\omega z} & -EH_s & 0 & 0 \\ -ES_\omega & -EI_{\omega x} & EI_{\omega z} & EI_{\omega\omega} & -EH_q & 0 & 0 \\ EH & EH_c & -EH_s & -EH_q & GJ & 0 & 0 \\ 0 & 0 & 0 & 0 & 0 & GA_{x\theta} & GA_{xz} \\ 0 & 0 & 0 & 0 & 0 & GA_{xz} & GA_{z\theta} \end{bmatrix} \begin{Bmatrix} \epsilon_{\theta r} \\ \kappa_{xr} \\ \kappa_{zr} \\ \dot{\tau}_r/R_0 \\ \tau_r \\ \gamma_{xr} \\ \gamma_{zr} \end{Bmatrix} \tag{33}$$

The stiffness in the first five rows and columns of this matrix were evaluated from a computer code developed by Woodson, Johnson, and Haftka (1993).

For structural models in which the effect of warping of the ring cross section is excluded the contribution of the bimoment, $M_{\omega r}$, to the ring virtual work in Eq. (31) is neglected. The fourth row and column of the stiffness matrix, Eq. (33), are ignored. Also, the contour warping function $\omega(x)$ is taken as zero.

CLASSICAL FORMULATIONS

Shell

The shell is modeled with Sanders' (1959) theory for thin shells. Define a generalized strain vector in terms of the shell strain measures by

$$\vec{\epsilon}_{shell} = [\epsilon_{xx}, \epsilon_{\theta\theta}, \gamma_{x\theta}, \kappa_{xx}, \kappa_{\theta\theta}, \kappa_{x\theta}]^T \tag{34}$$

The first five strain measures of the shell reference surface in Eq. (31) are related to the displacements by Eqs. (7-9), and the sixth strain measure, $\kappa_{x\theta}$, is given by

$$\kappa_{x\theta} = \frac{\partial \phi_\theta}{\partial x} + \frac{1}{R}\frac{\partial \phi_x}{\partial \theta} + \frac{1}{R}\phi_z \tag{35}$$

where the rotation about the normal, ϕ_z, is

$$\phi_z = \frac{1}{2}\left(\frac{\partial v}{\partial x} - \frac{1}{R}\frac{\partial u}{\partial \theta}\right) \tag{36}$$

and the rotations ϕ_x and ϕ_θ of the normal are given by Eqs. (13) and (14).

Define a generalized stress vector in terms of the stress resultants and couples of Sanders' theory by

$$\vec{\sigma}_{shell} = [N_{xx}, N_{\theta\theta}, N^s_{x\theta}, M_{xx}, M_{\theta\theta}, M^s_{x\theta}]^T \tag{37}$$

such that the internal virtual work is given by Eq. (22). Quantities $N^s_{x\theta}$ and $M^s_{x\theta}$ are the modified shear resultant and twisting moment resultant in the Sanders theory. Hooke's law for a laminated composite shell wall is

$$\vec{\sigma}_{shell} = H\vec{\epsilon}_{shell} \qquad H = \begin{bmatrix} A & B \\ B^T & D \end{bmatrix} \tag{38}$$

in which the 3×3 sub-matrices A, B and D are given by classical lamination theory (Jones, 1975). The external virtual work expressions for the classical shell theory are still given by Eqs. (26) and (27), but the rotations in Eqs. (27) are given by Eqs. (13) and (14).

Stringer

The stringer is modeled with Euler-Bernoulli beam theory thereby neglecting the transverse shear strain. Hence, equating γ_{zs} in Eq. (29) to zero results in the following expression for $\phi_{\theta s}$.

$$\phi_{\theta s} = -w'_s \tag{39}$$

It may be noted that neglecting the transverse shear strain would also modify the virtual work statement given by Eq. (28), and the third equation in the Hooke's law, Eq. (30), is neglected.

Ring

For classical formulations, the ring is modeled with Euler-Bernoulli beam theory thereby neglecting the transverse shear strains. Hence, equating γ_{xr} and γ_{zr} in Eq. (32) to zero results in the following expressions for the rotations ϕ_{xr} and ϕ_{zr}.

$$\phi_{xr} = \frac{1}{R_0}(v_r - \dot{w}_r) \qquad \phi_{zr} = -\frac{1}{R_0}\dot{u}_r \tag{40}$$

It may be noted that neglecting the transverse shear strains would also modify the virtual work statement given by Eq. (31), and the fifth and sixth equations in the Hooke's law, Eq. (33), are neglected.

DISPLACEMENT CONTINUITY

In order to maintain continuous deformation between the inside surface of the shell and stiffeners along their lines of contact, the following displacement continuity constraints are imposed:

Along the shell - stringer interface (i.e., $-l \leq x \leq l$, $\theta = 0$),

$$g_{xs} = u(x,0) - \frac{t}{2}\phi_x(x,0) - \left[u_s(x) + e_s\phi_{\theta s}(x)\right] = 0 \tag{41}$$

$$g_{zs} = w(x,0) - w_s(x) = 0 \tag{42}$$

Along the shell - ring interface (i.e., $x = 0$, $-\Theta \leq \theta \leq \Theta$),

$$g_{xr} = u(0,\theta) - \frac{t}{2}\phi_x(0,\theta) - \left[u_r(\theta) + e_r\phi_{\theta r}(\theta)\right] = 0 \tag{43}$$

$$g_{\theta r} = v(0,\theta) - \frac{t}{2}\phi_\theta(0,\theta) - \left[v_r(\theta) + e_r\phi_{xr}(\theta) - \omega_0\tau_r(\theta)\right] = 0 \tag{44}$$

$$g_{zr} = w(0,\theta) - w_r(\theta) = 0 \tag{45}$$

$$G_{\theta r} = -\frac{\partial w}{\partial x}\Big|_{x=0} - \phi_{\theta r}(\theta) = 0 \tag{46}$$

$$G_{zr} = \left[\frac{\partial v}{\partial x}\Big|_{x=0} - \frac{t}{2}\frac{\partial \phi_\theta}{\partial x}\Big|_{x=0}\right] - \left[\phi_{zr}(\theta) - \omega_1\tau_r(\theta)\right] = 0 \tag{47}$$

The variational form of these constraints are

$$\int_{-l}^{l} \left[\delta\lambda_{xs}g_{xs} + \delta\lambda_{zs}g_{zs}\right] dx = 0 \tag{48}$$

$$\int_{-\Theta}^{\Theta} \left[\delta\lambda_{xr}g_{xr} + \delta\lambda_{\theta r}g_{\theta r} + \delta\lambda_{zr}g_{zr} + \delta\Lambda_{\theta r}G_{\theta r} + \delta\Lambda_{zr}G_{zr}\right] (R_0 + e_r)\, d\theta = 0 \tag{49}$$

The constraint that the elongation of the shell at $\theta = 0$ and the elongation of the stringer are the same is

$$\delta Q\{[u(l,0) - u(-l,0)] - [u_s(l) - u_s(-l)]\} = 0 \tag{50}$$

DISPLACEMENTS, ROTATIONS, AND INTERACTING LOAD APPROXIMATIONS

The periodic portions of the displacements and rotations are represented by truncated Fourier Series having fundamental periods in the stringer and ring spacing. The non-periodic portions of the displacements due to axial stretching are represented by simple terms in x. The Fourier series reflect symmetry about the x-axis for the repeating unit. For the shell, displacements of the middle surface (see Fig. 3a) are represented as

$$u(x,\theta) = \frac{q_0 x}{2l} + \sum_{m=1}^{M}\sum_{n=0}^{N} u_{1mn} Sin(\alpha_m x) Cos(\beta_n \theta) + \sum_{m=1}^{M}\sum_{n=1}^{N} u_{2mn} Cos(\alpha_m x) Cos(\beta_n \theta) \tag{51}$$

$$v(x,\theta) = \sum_{m=0}^{M}\sum_{n=1}^{N} v_{1mn} Cos(\alpha_m x) Sin(\beta_n \theta) + \sum_{m=1}^{M}\sum_{n=1}^{N} v_{2mn} Sin(\alpha_m x) Sin(\beta_n \theta) \tag{52}$$

$$w(x,\theta) = \sum_{m=0}^{M}\sum_{n=0}^{N} w_{1mn} Cos(\alpha_m x) Cos(\beta_n \theta) + \sum_{m=1}^{M}\sum_{n=1}^{N} w_{2mn} Sin(\alpha_m x) Cos(\beta_n \theta) \tag{53}$$

and rotations of the normal are

$$\phi_x(x,\theta) = \sum_{m=1}^{M}\sum_{n=0}^{N} \phi_{x1mn} Sin(\alpha_m x) Cos(\beta_n \theta) + \sum_{m=1}^{M}\sum_{n=1}^{N} \phi_{x2mn} Cos(\alpha_m x) Cos(\beta_n \theta) \tag{54}$$

$$\phi_\theta(x,\theta) = \sum_{m=0}^{M}\sum_{n=1}^{N} \phi_{\theta 1mn} Cos(\alpha_m x) Sin(\beta_n \theta) + \sum_{m=1}^{M}\sum_{n=1}^{N} \phi_{\theta 2mn} Sin(\alpha_m x) Sin(\beta_n \theta) \tag{55}$$

in which $\alpha_m = \frac{m\pi}{l}$ and $\beta_n = \frac{n\pi}{\Theta}$ where m and n are non-negative integers. Note that some terms in the truncated Fourier Series of Eqs. (51-55) have been omitted.

The coefficients of the omitted terms are u_{200}, u_{2m0}, u_{20n}, w_{2m0}, ϕ_{x200}, ϕ_{x2m0}, and ϕ_{x20n}, in which $m = 1, 2, ..., M$ and $n = 1, 2, ..., N$. The rationale for their omission is discussed in the following sub-section. The displacements of the centroidal line of stringer (see Fig. 3b) are

$$u_s(x) = \frac{q_1 x}{2l} + \sum_{m=1}^{M} u_{s1m} Sin(\alpha_m x) + \sum_{m=1}^{M} u_{s2m} Cos(\alpha_m x) \tag{56}$$

$$w_s(x) = \sum_{m=1}^{M} w_{s1m} Sin(\alpha_m x) + \sum_{m=1}^{M} w_{s2m} Cos(\alpha_m x) \tag{57}$$

and the rotation of the normal of the stringer about the θ-axis is

$$\phi_{\theta s}(x) = \sum_{m=1}^{M} \phi_{\theta s1m} Sin(\alpha_m x) + \sum_{m=1}^{M} \phi_{\theta s2m} Cos(\alpha_m x) \tag{58}$$

where the coeffcients u_{s20} , w_{s20} and $\phi_{\theta s20}$ are omitted. Coefficient q_0 in the axial displacement field of the shell and q_1 in the axial displacement field of the stringer represent elongations of each respective element caused by either an axial mechanical load or due to close-end pressure vessel effects. The displacements of the reference circle of the ring (see Fig. 3c) are

$$u_r(\theta) = \sum_{n=1}^{N} u_{rn} Cos(\beta_n \theta) \tag{59}$$

$$v_r(\theta) = \sum_{n=1}^{N} v_{rn} Sin(\beta_n \theta) \tag{60}$$

$$w_r(\theta) = \sum_{n=0}^{N} w_{rn} Cos(\beta_n \theta) \tag{61}$$

and rotations are

$$\phi_{xr}(\theta) = \sum_{n=1}^{N} \phi_{xrn} Sin(\beta_n \theta) \tag{62}$$

$$\phi_{\theta r}(\theta) = \sum_{n=1}^{N} \phi_{\theta rn} Cos(\beta_n \theta) \tag{63}$$

$$\phi_{zr}(\theta) = \sum_{n=1}^{N} \phi_{zrn} Sin(\beta_n \theta) \tag{64}$$

where the coeffcients u_{r0} and $\phi_{\theta r0}$ are omitted. The distributions of the interacting loads, or Lagrange multipliers, are taken as

$$\lambda_{xs}(x) = \sum_{m=1}^{M} \lambda_{xs1m} Sin(\alpha_m x) + \sum_{m=1}^{M} \lambda_{xs2m} Cos(\alpha_m x) \tag{65}$$

$$\lambda_{zs}(x) = \sum_{m=1}^{M} \lambda_{zs1m} Sin(\alpha_m x) + \sum_{m=1}^{M} \lambda_{zs2m} Cos(\alpha_m x) \tag{66}$$

$$\lambda_{xr}(\theta) = \sum_{n=1}^{N} \lambda_{xrn} Cos(\beta_n \theta) \tag{67}$$

$$\lambda_{\theta r}(\theta) = \sum_{n=1}^{N} \lambda_{\theta rn} Sin(\beta_n \theta) \tag{68}$$

$$\lambda_{zr}(\theta) = \sum_{n=0}^{N} \lambda_{zrn} Cos(\beta_n \theta) \tag{69}$$

$$\Lambda_{\theta r}(\theta) = \sum_{n=1}^{N} \Lambda_{\theta rn} Cos(\beta_n \theta) \tag{70}$$

$$\Lambda_{zr}(\theta) = \sum_{n=1}^{N} \Lambda_{zrn} Sin(\beta_n \theta) \tag{71}$$

where the coefficients λ_{x2s0}, λ_{z2s0}, λ_{xr0}, and $\Lambda_{\theta r0}$ are omitted.

Terms Omitted in the Fourier Series

Terms omitted in the truncated Fourier Series for the displacements, rotations, and the interacting loads were determined from rigid body equilibrium conditions for the ring and stringer, and from displacement continuity conditions between the shell and the stiffeners. The external virtual work for the stringer and ring must vanish for any possible rigid body motions of these elements. For the stringer these rigid body motions are spatially uniform x-direction and z-direction displacements. (A rigid body rotation of the stringer in the x-z plane is not considered since this

motion would violate longitudinal periodicity of the repeating units.) Vanishing of the external virtual work for an arbitrary rigid body displacement of the stringer in the axial direction leads to the x-direction equilibrium equation

$$\int_{-l}^{l} \lambda_{xs}(x)\, dx = 0 \tag{72}$$

Similarly, the equilibrium equation for a rigid body displacement of the stringer in the z-direction is

$$\int_{-l}^{l} \lambda_{zs}(x)\, dx = 0 \tag{73}$$

If the ring is considered in its entirety, that is, as made up of an integer number of repeating units around its circumference, the rigid body motions that lead to non-trivial equilibrium conditions are a displacement in the x-direction and a rotation about an axis through the centeroid of the ring parallel to the x-direction. The x-direction equilibrium equation is

$$\int_{-\Theta}^{\Theta} \lambda_{xr}(\theta)\, (R_0 + e_r)\, d\theta = 0 \tag{74}$$

and the moment equilibrium equation about the x-axis is

$$\int_{-\Theta}^{\Theta} \lambda_{\theta r}(\theta)\, (R_0 + e_r)^2\, d\theta = 0 \tag{75}$$

Equilibrium Eqs. (72) to (74) imply that coefficients

$$\lambda_{xs20} = 0 \qquad \lambda_{zs20} = 0 \qquad \lambda_{xr0} = 0 \tag{76}$$

in the Fourier Series for the interacting loads, and these conditions have been taken into account in Eqs. (65) to (67). The sine series for $\lambda_{\theta r}$ given in Eq. (68) satisfies the equilibrium condition given in Eq. (75).

Consider the variational form of the constraints, Eqs. (48) and (49), for the spatially uniform components of the virtual interacting loads. These equations are

$$\Big[u_{200} - \frac{t}{2}\phi_{x200} + \sum_{n=1}^{N}(u_{20n} - \frac{t}{2}\phi_{x20n}) - (u_{s20} + e_s\phi_{\theta s20})\Big]\delta\lambda_{xs20} \;=\; 0 \qquad (77)$$

$$\Big[\sum_{n=0}^{N} w_{10n} - w_{s20}\Big]\delta\lambda_{zs20} \;=\; 0 \qquad (78)$$

$$\Big[u_{200} - \frac{t}{2}\phi_{x200} + \sum_{m=1}^{M}(u_{2m0} - \frac{t}{2}\phi_{x2m0}) - (u_{r0} + e_r\phi_{\theta r0})\Big]\delta\lambda_{xr0} \;=\; 0 \qquad (79)$$

Since these equations are satisfied on the basis that $\delta\lambda_{xs20} = 0$, $\delta\lambda_{zs20} = 0$ and $\delta\lambda_{xr0} = 0$, consistent with Eq. (76), the bracketed terms in Eqs. (77) to (79) do not necessarily vanish. The implication that these bracketed terms in Eqs. (77) to (79) do not vanish is that displacement continuity conditions are not satisfied pointwise. Pointwise continuity can be achieved by taking each Fourier coefficient appearing in the bracketed terms of Eqs. (77) to (79) to be individually zero. Fourier Series given in Eqs. (51), (54), (56), (58), (59), and (63) reflect this choice. Moreover, Fourier coefficients u_{200}, u_{s20}, and u_{r0} represent rigid body displacement in the axial direction for the shell, stringer, and ring, respectively, and setting them to zero can be justified on the basis that rigid body displacement does not contribute to the deformation of the structural elements. Since Fourier coefficient w_{s20} represents rigid body displacement of the stringer in the z-direction, it would seem that it should be set to zero as well. However, to maintain continuity between the stringer and the shell in the z-direction, we impose the condition

$$\sum_{n=0}^{N} w_{10n} - w_{s20} \;=\; 0 \qquad (80)$$

to determine w_{s20} after obtaining the solution for the displacement components that deform the shell; i.e., Fourier coefficients w_{10n}, $n = 1, ..., N$, are taken to be non-zero independent degrees of freedom since the stringer coefficient w_{s20} is not a part of the solution vector.

Finally, consider the constraint equation associated with $\delta\Lambda_{\theta r0}$, the spatially uniform component of the interacting moment intensity, which was omitted in the series given by Eq. (70). Derived from Eq. (49), this constraint equation is

$$\Big[\sum_{m=1}^{M} \alpha_m w_{2m0} + \phi_{\theta r0}\Big]\delta\Lambda_{\theta r0} \;=\; 0 \tag{81}$$

We equated the constant component of the twist, $\phi_{\theta r0}$, to zero from the considerations associated with Eq. (79). Consequently, a non-zero value of the constant component of the interacting moment intensity, $\Lambda_{\theta r0} \neq 0$, would not contribute to the equilibrium of the ring, since $\Lambda_{\theta r0}$ and $\phi_{\theta r0}$ are conjugate variables in the external work for the ring (refer to Eq. (31)). Since $\phi_{\theta r0} = 0$, it is necessary that $\Lambda_{\theta r0} = 0$ to achieve consistent conditions for the torsional and out-of-plane bending equilibrium of the ring. With $\delta\Lambda_{\theta r0} = 0$ in Eq. (81), the bracketed term does not necessarily vanish, and as a result pointwise rotational continuity betwen the shell and the ring is not assured. Pointwise rotational continuity is achieved if we take the coefficients $w_{2m0} = 0,\ m = 1, ..., M$, as was done in the Fourier Series for the normal displacement of the shell given by Eq. (53).

DISCRETE EQUATIONS AND THEIR SOLUTION

Transverse Shear Deformation Model

The discrete displacement vector for the shell is the $(10MN + 3M + 3N + 2) \times 1$ vector

$$\hat{u}_{shell} = \left[\hat{u}_0^T, \hat{u}_1^T, ..., \hat{u}_M^T\right]^T \tag{82}$$

in which subvectors are

$$\hat{u}_0 = \left[q_0, w_{100}, v_{101}, w_{101}, \phi_{\theta 101}, ..., v_{10N}, w_{10N}, \phi_{\theta 10N}\right]^T \tag{83}$$

$$\begin{aligned}\hat{u}_m = \big[&u_{1m0}, w_{1m0}, \phi_{x1m0}, u_{1m1}, u_{2m1}, v_{1m1}, v_{2m1}, w_{1m1}, w_{2m1}, \phi_{x1m1}, \phi_{x2m1},\\ &\phi_{\theta 1m1}, \phi_{\theta 2m1}, ..., u_{1mN}, u_{2mN}, v_{1mN}, v_{2mN}, w_{1mN}, w_{2mN}, \phi_{x1mN},\\ &\phi_{x2mN}, \phi_{\theta 1mN}, \phi_{\theta 2mN}\big]^T\end{aligned} \tag{84}$$

where $m = 1, ..., M$

The $(6M + 1) \times 1$ discrete displacement vector for the stringer and $(6N + 1) \times 1$ vector for the ring are

$$\hat{u}_{str} = \left[q_1, u_{s11}, u_{s21}, w_{s11}, w_{s21}, \phi_{\theta s11}, \phi_{\theta s21}, ..., u_{s1M}, u_{s2M}, \right. \\ \left. \hat{w}_{s1M}, w_{s2M}, \phi_{\theta s1M}, \phi_{\theta s2M}\right]^T \tag{85}$$

$$\hat{u}_{ring} = \left[w_{r0}, u_{r1}, v_{r1}, w_{r1}, \phi_{\theta r1}, \phi_{xr1}, \phi_{zr1}, ..., u_{rN}, v_{rN}, w_{rN}, \phi_{\theta rN}, \phi_{xrN}, \phi_{zrN}\right]^T \tag{86}$$

in which the term w_{s0} for the stringer has been omitted as discussed in reference to Eq. (80). The $4M \times 1$ discrete interacting loads vector for the shell-stringer interface and $(5N + 1) \times 1$ vector for the shell-ring interface are

$$\hat{\lambda}_{str} = \left[\lambda_{xs11}, \lambda_{xs21}, \lambda_{zs11}, \lambda_{zs21}, ..., \lambda_{xs1M}, \lambda_{xs2M}, \lambda_{zs1M}, \lambda_{zs2M}\right]^T \tag{87}$$

$$\hat{\lambda}_{ring} = \left[\lambda_{zr0}, \lambda_{xr1}, \lambda_{\theta r1}, \lambda_{zr1}, \Lambda_{\theta r1}, \Lambda_{zr1}, ..., \lambda_{xrN}, \lambda_{\theta rN}, \lambda_{zrN}, \Lambda_{\theta rN}, \Lambda_{zrN}\right]^T \tag{88}$$

Classical Model

The discrete displacement vector for the shell is the $(6MN + 2M + 2N + 2) \times 1$ vector

$$\hat{u}_{shell} = \left[\hat{u}_0^T, \hat{u}_1^T, ..., \hat{u}_M^T\right]^T \tag{89}$$

in which subvectors are

$$\hat{u}_0 = \left[q_0, w_{100}, v_{101}, w_{101}, ..., v_{10N}, w_{10N}\right]^T \tag{90}$$

$$\hat{u}_m = \left[u_{1m0}, w_{1m0}, u_{1m1}, u_{2m1}, v_{1m1}, v_{2m1}, w_{1m1}, w_{2m1}, ..., u_{1mN}, u_{2mN}, \right. \\ \left. v_{1mN}, v_{2mN}, w_{1mN}, w_{2mN}\right]^T \tag{91}$$

where $m = 1, ..., M$

The $(4M + 1) \times 1$ discrete displacement vector for the stringer and $(4N + 1) \times 1$ vector for the ring are

$$\hat{u}_{str} = \left[q_1, u_{s11}, u_{s21}, w_{s11}, w_{s21}, ..., u_{s1M}, u_{s2M}, w_{s1M}, w_{s2M}\right]^T \tag{92}$$

$$\hat{u}_{ring} = \left[w_{r0}, u_{r1}, v_{r1}, w_{r1}, \phi_{\theta r1}, ..., u_{rN}, v_{rN}, w_{rN}, \phi_{\theta rN}\right]^T \tag{93}$$

The $4M \times 1$ discrete interacting loads vector for the shell-stringer interface and $(5N+1) \times 1$ vector for the shell-ring interface are the same as for the shear deformation model and are given by Eqs. (87) and (88).

The approximations in Eqs. (51) through (64) for the displacements and Eqs. (65) through (71) for the interacting loads are substituted into the virtual work functionals for each structural element, and also substituted into the variational form of displacement continuity constraints. Then integration over the space is performed. (The test space of virtual displacements and the virtual interacting loads is the same space used for the approximations in Eqs. (51-71).) This process results in a $10MN+13M+14N+6$ system of equations for the transverse shear deformation model and $6MN + 10M + 11N + 6$ system of equations for the classical model, governing the displacements and the interacting loads. The governing equations are of the form

$$\begin{bmatrix} K_{11} & 0 & 0 & B_{11} & B_{12} & B_{13} \\ 0 & K_{22} & 0 & B_{21} & 0 & B_{23} \\ 0 & 0 & K_{33} & 0 & B_{32} & 0 \\ B_{11}^T & B_{21}^T & 0 & 0 & 0 & 0 \\ B_{12}^T & 0 & B_{32}^T & 0 & 0 & 0 \\ B_{13}^T & B_{23}^T & 0 & 0 & 0 & 0 \end{bmatrix} \begin{Bmatrix} \hat{u}_{shell} \\ \hat{u}_{str} \\ \hat{u}_{ring} \\ \hat{\lambda}_{str} \\ \lambda_{ring} \\ Q \end{Bmatrix} = \begin{Bmatrix} F_{11} \\ 0 \\ 0 \\ 0 \\ 0 \\ 0 \end{Bmatrix} \tag{94}$$

in which sub-matrices K_{11}, K_{22} and K_{33} are the stiffness matrices for the shell, stringer, and ring, respectively. The sub-matrices $B_{ij}, i, j = 1, 2, 3$, in Eq. (94) are determined from the external virtual work terms involving the interacting loads, and the constraint Eqs. (48) to (50). The vector on the right-hand-side of Eq. (94) is the force vector, determined from the external virtual work terms involving pressure. The constraint equations correspond to the last three rows of the partitioned matrix in Eq. (94). Equation (94) is first solved for the displacements in terms of interacting loads, then this solution is substituted into the constraint equations to determine the interacting loads. Thus, the total solution is obtained.

NUMERICAL EXAMPLE

Data for the numerical example are representative of a large transport fuselage structure. The shell radius $R = 122.0$ in., frame spacing $2l = 22$ in., and stringer spacing $2R\Theta = 15.0$ in. The shell wall is a 13-ply $[\pm 45, 90, 0, \pm 60, 90, \pm 60, 0, 90, \pm 45]_T$ laminate of graphite-epoxy AS4/938 tow prepreg with total thickness of 0.0962 in. The ply thickness is 0.0074 in., and the lamina material properties are assumed to be $E_1 = 19.21 \times 10^6 lb/in.^2$, $E_2 = 1.36 \times 10^6 lb/in.^2$, $G_{12} = G_{13} = G_{23} = 0.72 \times 10^6 lb/in.^2$, and $\nu_{12} = 0.32$. For the transverse shear deformation model, the shell wall stiffness sub-matrices of Eq. (23) are computed using these ply data and the expressions for the stiffness elements given in the Appendix. The numerical results are

$$A = \begin{bmatrix} 0.5774 & 0.2619 & 0 \\ 0.2619 & 0.9766 & 0 \\ 0 & 0 & 0.2889 \end{bmatrix} \times 10^6 \ lb/in.$$

$$B = \begin{bmatrix} 3.893 & 0 & 0.1847 & 0.1847 \\ 0 & -5.043 & -0.2213 & 0.2213 \\ 0 & -0.443 & -1.1351 & 1.1351 \end{bmatrix} lb$$

$$D = \begin{bmatrix} 474.937 & 256.071 & 45.074 & 0 \\ 256.071 & 615.194 & 54.003 & -0.47 \times 10^{-5} \\ 45.074 & 54.003 & 276.965 & -0.75 \times 10^{-5} \\ 0 & -0.47 \times 10^{-5} & -0.75 \times 10^{-5} & 0.75 \times 10^{-5} \end{bmatrix} lb\ in.$$

and elements of the transverse shear stiffness matrix in Eq. (24) are

$$A_{44} = A_{55} = 0.69264 \times 10^5 \ lb/in., \qquad A_{45} = 0$$

The bending and stretching-bending coupling sub-matrices for classical lamination theory, Eq. (38), are given by

$$D = \begin{bmatrix} 474.937 & 256.071 & 0 \\ 256.071 & 615.194 & 0 \\ 0 & 0 & 276.965 \end{bmatrix} lb\ in. \qquad B = 0$$

The extensional stiffness sub-matrix A is the same for classical theory and the transverse shear deformation theory.

Cross sections of the stiffeners and their dimensions are shown in Fig. 4. The stringer is an inverted hat section laminated from twelve plies of AS4/938 graphite-epoxy tow prepreg with a $[\pm 45, 0_2, 90, \pm 15, 90, 0_2, \pm 45]_T$ lay up and total thickness of 0.0888 in. The stiffnesses in Hooke's law for the stringer in Eq. (30) are

$$(EA)_s = 0.6675 \times 10^7 lb, \quad (EI)_s = 0.2141 \times 10^7 lb\ in.^2, \quad (GA)_s = 0.843 \times 10^6 lb$$

We assume a 2-D braided frame consisting of 0^o and 90^o tows. The wall thickness is 0.141 inches, and the elastic modulii are assumed to be $E_1 = 7.76 \times 10^6 lb/in.^2$, $E_2 = 8.02 \times 10^6 lb/in.^2$, $G_{12} = G_{13} = G_{23} = 1.99 \times 10^6 lb/in.^2$, and $\nu_{12} = 0.187$. Using the ring material properties and the cross-sectional dimensions, the stiffness matrix for the ring in Eq. (33) is computed. The non-zero stiffnesses are

$$EA = 0.9088 \times 10^7 lb, \quad EI_{xx} = 3.915 \times 10^7 lb\ in.^2, \quad EI_{zz} = 0.1867 \times 10^7 lb\ in.^2$$

$$EI_{zx} = 0.2993 \times 10^7 lb\ in.^2, \quad EI_{\omega x} = -1.322 \times 10^7 lb\ in.^3, \quad GJ = 0.1346 \times 10^5 lb\ in.^2$$

$$EI_{\omega\omega} = 1.705 \times 10^7 lb\ in.^4, \quad EI_{\omega z} = -0.1865 \times 10^6 lb\ in.^3$$

$$GA_{x\theta} = GA_{z\theta} = 0.2396 \times 10^7\ lb$$

All the results presented are for an internal pressure $p = 10$ psi, and the Fourier series are truncated at twenty-four terms in the x- and θ-directions ($M = N = 24$).

RESULTS AND DISCUSSION

Interacting Load Distributions

The distributions of the interacting load intensities between the stiffeners and the shell are shown in Figs. 5 through 11. The effects of transverse shear deformations and of warping of the ring's cross section due to torsion on the magnitudes of the interacting line loads are summarized in Table 1. For the component λ_{xs} tangent to the stringer (Fig. 5), there are only small differences in the distributions as predicted by the four structural models. However, the peak value of the component

normal to the stringer, λ_{zs}, is reduced in the transverse shear deformation models with respect to its peak value in the classical models (Fig. 6 and Table 1).

The distributions of axial force intensity, λ_{xr}, between the ring and shell predicted by the classical and shear deformation models with warping are nearly the same (Fig. 7). However, the distributions of this force intensity predicted by the classical and shear deformation models without warping have significant differences. Thus, this interacting load intensity is more sensitive to the inclusion or exclusion of warping of the ring cross section into the structural model. As shown in Fig. 8, the differences in the results for circumferential force intensity, $\lambda_{\theta r}$, between the ring and shell from the four models are small, except in the vicinity of the stiffener intersection where the effects of including the transverse shear deformation into the models are manifested. However, the differences in $\lambda_{\theta r}$ occur over one wave length of the highest frequency i.e., $\Delta\theta/\Theta = 2/24$. Differences occuring over the shortest wavelength may not be significant; more terms in the Fourier series are required to verify this. The distributions of the normal force intensity, λ_{zr}, between the ring and shell predicted by the four models are essentially the same (Fig. 9). The distributions of the circumferential moment component, $\Lambda_{\theta r}$, predicted by the classical models have higher magnitudes as compared to shear deformation models (Fig. 10 and Table 1). Also note the change in sign of $\Lambda_{\theta r}$ distributions in the vicinity of the joint as a result of inclusion of warping into the models. The classical theory predicts much larger magnitudes of normal moment component, Λ_{zr}, compared to the transverse shear deformation theory for the models in which warping is included (Fig. 11 and Table 1). However, the reverse is true for the structural models with no warping. Also, there is a change in sign in the distributions of Λ_{zr} for classical models with and without warping effects.

The distribution of the normal component of the traction across the width of the attachment flange of the ring is represented by line force intensity λ_{zr} and line moment intensity $\Lambda_{\theta r}$. The values of λ_{zr} are nearly the same in the classical and transverse shear deformation models (Fig. 9), but magnitudes of $\Lambda_{\theta r}$ are

substantially *decreased* in the transverse shear deformation models with respect to the classical models (Fig. 10). Thus, the asymmetry of the normal traction across the flange width of the ring is *decreased* in the transverse shear deformation models with respect to the classical models.

The distribution of the circumferential component of the traction across the width of the attachment flange of the ring is represented by line force intensity $\lambda_{\theta r}$ and line moment intensity Λ_{zr}. The values of $\lambda_{\theta r}$ are nearly the same in the classical and transverse shear deformation models (Fig. 8). However, the magnitude of Λ_{zr} is substantially *increased* in the transverse shear deformation model with respect to the classical model with warping excluded, and is substantially *decreased* in the transverse shear deformation model with respect to the classical model with warping included (Fig. 11). Thus, the asymmetry of the circumferential traction across the flange width of the ring is *increased* in the transverse shear deformation model with respect to the classical model without warping, and is *decreased* in the transverse shear deformation model with respect to the classical model with warping.

For the stiffened shell configuration with asymmetrical cross section ring, the inclusion of transverse shear deformation and warping of ring cross section into the analyses influences the distributions and magnitudes of interacting line load components λ_{zs}, λ_{xr}, $\lambda_{\theta r}$, $\Lambda_{\theta r}$, and Λ_{zr}. The distributions of interacting line load components λ_{xs} and λ_{zr} remain essentially the same. The cause of sensitivity to transverse shear deformations is two-fold: First, the tangential displacements of the shell along the contact lines are *de-coupled* from the out-of-plane rotations of the reference surface of the shell, and for the stiffeners the longitudinal displacements along the contact lines are *de-coupled* from the rotations of the longitudinal reference axes. Second, in the transverse shear deformation model, the torsional rotation of the ring at the shell-stringer-ring joint is *de-coupled* from the in-plane bending rotation of the stringer at the joint, thereby allowing for increased joint flexibility. In the classical model, the torsional rotation of the ring at the joint is constrained to be the same as the bending rotation of the stringer (see Fig. 12). The values

of these joint rotations for the four structural models are given in Table 2. Notice from Table 2 that the sense of the rotation changes if warping is included, and that the transverse shear deformation results in a torsional rotation of the ring that is about twice as much as the bending rotation of the stringer.

Resultants at the Stiffener Intersection

The interacting line load intensities acting on the inside of the shell wall can be resolved into a resultant at the stiffener intersection ($x = \theta = 0$). In general this resultant consists of a force with components F_x, F_θ and F_z, and a couple with moment components C_x, C_θ and C_z. These components are shown in their positive sense on the inside of the shell wall in Fig. 13. The components of the resultant force vector are defined by

$$F_x = \int_{-l}^{l} \lambda_{xs}\, dx + \int_{-\Theta}^{\Theta} \lambda_{xr}\, (R - \frac{t}{2})\, d\theta \tag{95}$$

$$F_\theta = \int_{-\Theta}^{\Theta} \left[\lambda_{\theta r}\, Cos\theta + \lambda_{zr}\, Sin\theta\right]\, (R - \frac{t}{2})\, d\theta \tag{96}$$

$$F_z = \int_{-l}^{l} \lambda_{zs}\, dx + \int_{-\Theta}^{\Theta} \left[\lambda_{zr}\, Cos\theta - \lambda_{\theta r}\, Sin\theta\right]\, (R - \frac{t}{2})\, d\theta, \tag{97}$$

and the components of the moment resultant of the couple are

$$C_x = \int_{-\Theta}^{\Theta} \left[\lambda_{zr} Sin\theta - (1 - Cos\theta)\lambda_{\theta r}\right]\, (R - \frac{t}{2})^2\, d\theta \tag{98}$$

$$C_\theta = -\int_{-l}^{l} x\lambda_{zs} dx + \int_{-\Theta}^{\Theta} \left[-\lambda_{xr}(1 - Cos\theta)(R - \frac{t}{2}) + \Lambda_{\theta r} Cos\theta + \Lambda_{zr} Sin\theta\right](R - \frac{t}{2}) d\theta \tag{99}$$

$$C_z = \int_{-\Theta}^{\Theta} \left[-\lambda_{xr}(R - \frac{t}{2}) Sin\theta - \Lambda_{\theta r} Sin\theta + \Lambda_{zr}\, Cos\theta\right]\, (R - \frac{t}{2})\, d\theta \tag{100}$$

It is found that substituting for interacting load approximations given by Eqs. (65-71) into Eqs. (95-100), and performing the line integrals results in components $F_x = F_\theta = C_x = C_z = 0$. Thus, at the stiffener intersection, the only non-zero resultants are a radial force resultant, F_z, and a circumferential moment resultant C_θ (refer Fig. 13). In Eq. (99) the circumferential moment component, C_θ, consists of two line integrals; first integral being the contribution of shell-stringer interacting loads, and second representing the contributions of shell-ring interacting loads. The contribution to the radial force resultant F_z in Eq. (97) comes only from the shell-ring interacting load intensitites since the resultant from the stringer vanishes by Eq. (73).

The values of the radial force and circumferential moment resultants are computed using Eqs. (97) and (99) for the four structural models under consideration, and are given in Table 3. The differences predicted by the four structural models in the magnitudes of the radial force resultant F_z are very small, and are within 0.4% of each other. There are substantial differences in the magnitudes of circumferential component of the moment predicted by the four models. The values of C_θ predicted by the models with warping included are much larger than those predicted by the models without warping effects. The individual contributions of the stringer and ring to C_θ are also affected by the change in the model as shown in Table 3. It may be noted that C_θ is more sensitive to the effect of warping than to transverse shear deformation.

Singular Behavior at the Joint

In Table 1 the comparison of peak values of the interacting line load intensities is meant to convey the influences of transverse shear deformations and warping in the structural modeling. The peak values of components λ_{zs}, λ_{xr}, λ_{zr}, and $\Lambda_{\theta r}$ occur at the joint, but these peak values do not exhibit convergence with an increasing number of terms retained in the Fourier series. It appears that these components are singular at the joint. However, the resultants F_z and C_θ determined from these

line load intensities were found to converge quite rapidly. See Johnson and Rastogi (1994) for further discussion of this point.

Stiffener Actions

The distributions of the force and moment resultants in the stiffeners are shown in Figs. 14 through 19. The stringer axial force and bending moment distributions (Fig. 14) are slightly asymmetric about the origin. The bending moment distributions in the stringer are more sensitive to the change in models as compared to the axial force distributions. The distribution of stringer shear force, V_{zs}, is shown in Fig. 15, and it is asymmetric about the origin. Only small differences are predicted by the four structural models in the distribution of V_{zs}.

The distributions of the circumferential force and in-plane bending moment in the ring are shown in Fig. 16. The differences in these distributions predicted by the four models are very small. The distributions in-plane shear force, V_{zr}, in the ring predicted by the four structural models have negligible differences, as shown in Fig. 17. The out-of-plane bending moment M_{zr} and torque T_r in the ring are more sensitive to the change in models as shown Fig. 18. The distributions of the out-of-plane bending moment are symmetric about the origin, and their magnitudes predicted by the models with warping included are substantially larger as compared to the magnitudes predicted by the models without warping. The distributions of total torque, T_r $(= T_{sr} - \dot{M}_{\omega r}/R_0)$, are antisymmetric about the origin. As shown in Fig. 18, the torque has reduced magnitudes in the transverse shear deformation model compared to the classical model when warping is included. The torque predicted by the models without warping is St. Venant's torque T_{sr}, and this is negligible as shown in Fig. 18. The distributions of out-of-plane shear force, V_{xr}, in the ring are shown in Fig. 19, and these distributions are antisymmetric about the origin. The magnitudes of V_{xr} predicted by the transverse shear deformation model are larger compared to the classical model when warping is included. However the reverse is true for the V_{xr} distributions without warping. The distributions for

$M_{\theta s}$, V_{zs}, M_{zr}, T_r and V_{xr} shown in Figs. 14, 15, 18 and 19, respectively, indicate that these stiffener actions are sensitive to both transverse shear deformations and warping deformations.

Shell Response

The distribution of the normal displacement along x-curve midway between the stringers ($\theta = -\Theta$), and along the θ-curve midway between the rings ($x = -l$), are shown in Fig. 20. As depicted in this figure, there is a negligible difference between the results from the transverse shear deformation model and classical model (warping of the ring is included in both models). Also, there is negligible difference in the axial and circumferential normal strain distributions between the two models as shown in Figs. 21 and 22. Thus, the normal displacement and in-plane normal strains for the shell are not significantly influenced by the inclusion of either transverse shear deformations or warping deformation of the ring into the structural models, in part because the shell is very thin for the example studied.

A Ring with Symmetric Cross Section

As a benchmark for comparing transverse shear deformation model with the classical model, analyses were performed for a ring with symmetric cross section. In this case the changes made to the numerical example under discussion are to set the bending-coupling stiffeness EI_{zx}, the out-of-plane bending to warping coupling stiffness $EI_{\omega x}$, and the contour warping function parameter ω_0 of the ring, all to zero. Consequently, the θ-axis, as well as the x-axis, are axes of symmetry for the repeating unit in terms of geometry, load, and material properties. Symmetry about the θ-axis implies there is no out-of-plane bending and torsion of the ring; i.e., $u_r(\theta) = \phi_{\theta r}(\theta) = \phi_{zr}(\theta) = \lambda_{xr}(\theta) = \Lambda_{\theta r}(\theta) = \Lambda_{zr}(\theta) = 0$ for $-\Theta \leq \theta \leq \Theta$. Thus, for the symmetrical section stiffeners only the interacting line load components tangent and normal to the stiffeners are non-zero. Since the internal pressure loading is symmetric, warping of the ring cross section does not play any role in the analyses.

The distributions of the tangential interacting load intensity between the shell and ring are shown in Fig. 23. The differences in the results from the two models are small except in the vicinity of the stiffener intersection. The peak magnitude of $\lambda_{\theta r}$ in the transverse shear deformation model is smaller than the peak value for $\lambda_{\theta r}$ in the classical model (50.8 lb/in versus 64.5 lb/in.). However, this difference occurs over one wave length of the highest harmonic retained in the analysis, and may not be significant. The distributions of the tangential and normal interacting load intensities between the shell and stringer, and the normal load intensity between the shell and ring are not significantly different in the two models.

For a symmetrical cross section ring, in Eqs. (95) through (100) $F_x = F_\theta = C_x = C_\theta = C_z = 0$. The only non-zero component of the force resultant is the radial force F_z. The values of F_z computed from the classical and transverse shear deformation models are -563.72 lb. and -561.89 lb., respectively.

CONCLUDING REMARKS

A unit cell model of an internally pressurized, long circular cylindrical shell stiffened on the inside by a regular arrangement of identical stringers and identical rings is analyzed. The ring is assumed to have an open asymmetrical cross section, and the stringer is assumed to have a symmetric section. The asymmetrical section ring significantly complicated the analysis of the unit cell, since symmetry about the plane of the ring is lost. Out-of-plane bending and torsion of the ring occur as well as a rotation of the shell-stringer-ring joint about the circumferential axis of the ring. Mathematical formulations for the linear elastic response presented in this work include the effects of transverse shear deformations and of out-of-plane warping of the ring's asymmetrical cross section due to torsion. Closed-end pressure vessel effects are included in the analyses. Data representative of a large transport aircraft are used in the numerical example.

For the stiffened shell configuration with an asymmetrical cross section ring, the inclusion of transverse shear deformation and warping of ring's cross section into

the analyses influences the distributions and magnitudes of interacting line load components between the shell wall and stiffeners (Table 1), and the stiffener actions (see Figs. 14 and 18). However, the normal displacement and in-plane normal strains for the shell are not significantly different in the four structural models. The cause of sensitivity to transverse shear deformations can be attributed to the *decoupling* of the torsional rotation of the ring at the shell-stringer-ring joint from the in-plane bending rotation of the stringer at the joint, thereby allowing for increased joint flexibility. In the classical model, the torsional rotation of the ring at the joint is constrained to be the same as the bending rotation of the stringer (see Fig. 12 and Table 2). The inclusion of warping of the ring's cross section due to torsion into the analyses causes the magnitude of the circumferential component of the moment resultant of the interacting line loads, C_θ, to increase substantially (see Table 3).

ACKNOWLEDGMENT

This research is supported by NASA Grant NAG-1-537, and Dr. James H. Starnes, Jr., NASA Langley Research Center is the technical monitor.

REFERENCES

Hoff, N. J. (1945). The applicablity of Saint-Venant's principle to airplane structures. *Journal of Aeronautical Science*, Vol. 12, pp. 455-460.

Ilcewicz, L. B., Smith, P. J., and Horton, R. E. (1992). Advanced composites fuselage technology. *Proceedings of the Third NASA/DoD Advanced Composites Technology Conference*, NASA CP-3178, pp. 97-156.

Jackson, A. C. (1994). Development of textile composite preforms for aircraft structures. *Proceedings of the AIAA/ASME/ASCE/AHS/ASC 35th Structures, Structural Dynamics and Materials Conference* (Hilton Head, SC), Part 2, AIAA, Washington, D.C., April, pp. 1008-1012.

Jackson, A. C., Campion, M. C., and Pei, G. (1984). Study of utilization of advanced composites in fuselage structures of large transports. *NASA Contractor Report 172404*, Contract NAS1-17415, September.

Johnson, E. R., and Rastogi, N. (1994). Interacting loads in an orthogonally stiffened composite cylindrical shell. *Proceedings of the AIAA/ASME/ASCE/AHS/ASC 35th Structures, Structural Dynamics and Materials Conference* (Hilton Head, SC), Part 5, AIAA, Washington, D.C., April, pp. 2607-2620.

Jones, R. M. (1975). *Mechanics of Composite Materials*, Scripta Book Co., Washington DC, pp. 51, 154, 155.

Novozhilov, V. V. (1964). *Thin Shell Theory*, Noordhoff Ltd., The Netherlands, p. 23.

Sanders, J. L. (1959). An improved first approximation theory for thin shells. *NASA Technical Report R-24*, June.

Swanson, G. D., Ilcewicz, L. B., Walker, T. H., Graesser, D., Tuttle, M., and Zabinsky, Z. (1992). Local design optimization for composite transport fuselage crown panels. *Proceedings of the Second NASA/DoD Advanced Composites Technology Conference*, NASA CP-3154, pp. 243-262.

Wang, J. T-S., and Hsu, T-H. (1985). Discrete analysis of stiffened composite cylindrical shells. *AIAA Journal*, Vol. 23, No. 11, pp. 1753-1761.

Woodson, M. B., Johnson, E. R., and Haftka, R. T. (1993). A Vlasov theory for laminated composite circular beams with thin-walled open sections. *Proceedings of the AIAA/ASME/ASCE/AHS/ASC 34th Structures, Structural Dynamics and Materials Conference* (LaJolla, CA), Part 5, AIAA, Washington, D.C., April, pp. 2742-2760.

Appendix

ELEMENTS OF STIFFNESS MATRIX FOR A CYLINDRICAL SHELL BASED ON TRANSVERSE SHEAR DEFORMATION THEORY

Based on the transverse shear deformation theory, the elements A_{ij}, B_{ij}, and D_{ij} of the stiffness matrices, in Eqs. (23) and (24) for the constitutive law for a laminated shell wall, are given by

$$A_{11} = \int_t \bar{Q}_{11}(1 + \frac{z}{R})dz$$

$$A_{12} = \int_t \bar{Q}_{12}dz$$

$$A_{16} = \int_t \bar{Q}_{16}dz$$

$$A_{22} = \int_t \bar{Q}_{22}(1 + \frac{z}{R})^{-1}dz$$

$$A_{26} = \int_t \bar{Q}_{26}(1 + \frac{z}{R})^{-1}dz$$

$$A_{66} = \int_t \bar{Q}_{66}(1 + \frac{z}{R})^{-1}dz$$

$$B_{11} = \int_t \bar{Q}_{11}z(1 + \frac{z}{R})dz$$

$$B_{12} = \int_t \bar{Q}_{12}zdz$$

$$B_{16}^1 = \int_t \bar{Q}_{16}z(1 + \frac{z}{R})dz$$

$$B_{16}^2 = \int_t \bar{Q}_{16}\frac{z^2}{2R}dz$$

$$B_{22} = \int_t \bar{Q}_{22}z(1 + \frac{z}{R})^{-1}dz$$

$$B_{26}^1 = \int_t \bar{Q}_{26}z(1 + \frac{z}{2R})(1 + \frac{z}{R})^{-1}dz$$

$$B_{26}^2 = \int_t \bar{Q}_{26}\frac{z^2}{2R}(1 + \frac{z}{R})^{-1}dz$$

$$B_{61} = \int_t \bar{Q}_{16}zdz$$

$$B_{62} = \int_t \bar{Q}_{16}z(1 + \frac{z}{R})^{-1}dz$$

$$B_{66}^{1} = \int_t \bar{Q}_{66} z (1 + \frac{z}{2R})(1 + \frac{z}{R})^{-1} dz$$

$$B_{66}^{2} = \int_t \bar{Q}_{66} \frac{z^2}{2R} (1 + \frac{z}{R})^{-1} dz$$

$$D_{11} = \int_t \bar{Q}_{11} z^2 (1 + \frac{z}{R}) dz$$

$$D_{12} = \int_t \bar{Q}_{12} z^2 dz$$

$$D_{16}^{1} = \int_t \bar{Q}_{16} z^2 (1 + \frac{z}{R}) dz$$

$$D_{16}^{2} = \int_t \bar{Q}_{16} \frac{z^3}{2R} dz$$

$$D_{22} = \int_t \bar{Q}_{22} z^2 (1 + \frac{z}{R})^{-1} dz$$

$$D_{26}^{1} = \int_t \bar{Q}_{26} z^2 (1 + \frac{z}{2R})(1 + \frac{z}{R})^{-1} dz$$

$$D_{26}^{2} = \int_t \bar{Q}_{26} \frac{z^3}{2R} (1 + \frac{z}{R})^{-1} dz$$

$$D_{66}^{11} = \int_t \bar{Q}_{66} z^2 (1 + \frac{z}{2R})^{2} (1 + \frac{z}{R})^{-1} dz$$

$$D_{66}^{12} = \int_t \bar{Q}_{66} \frac{z^3}{2R} (1 + \frac{z}{2R})(1 + \frac{z}{R})^{-1} dz$$

$$D_{66}^{22} = \int_t \bar{Q}_{66} \frac{z^4}{4R^2} (1 + \frac{z}{R})^{-1} dz$$

where $\bar{Q}_{ij}$ are the transformed reduced stiffnesses given in the text by Jones (1975).

Based on the assumption of constant transverse shear strain distribution through the thickness, the transverse shear stiffnesses are given by

$$A_{44} = \int_t C_{44} (1 + \frac{z}{R}) dz$$

$$A_{45} = \int_t C_{45} dz$$

$$A_{55} = \int_t C_{55} (1 + \frac{z}{R})^{-1} dz$$

where

$$C_{44} = G_{13} Cos^2 \alpha + G_{23} Sin^2 \alpha$$

$$C_{45} = (G_{13} - G_{23}) Cos\alpha Sin\alpha$$

$$C_{55} = G_{23} Cos^2\alpha + G_{13} Sin^2\alpha$$

in which α is the ply orientation angle.

Based on the assumption of constant transverse shear stress distribution through the thickness, the transverse shear stiffnesses are given by

$$A_{44} = \frac{k_{22}}{k} \qquad A_{45} = -\frac{k_{12}}{k} \qquad A_{55} = \frac{k_{11}}{k}$$

in which $k = k_{11}k_{22} - k_{12}^2$. The coefficients k_{ij} are given by

$$k_{11} = \frac{1}{t^2} \int_t c_{44} (1 + \frac{z}{R})^{-1} dz$$

$$k_{12} = \frac{1}{t^2} \int_t c_{45} dz$$

$$k_{22} = \frac{1}{t^2} \int_t c_{55} (1 + \frac{z}{R}) dz$$

where

$$c_{44} = \frac{Cos^2\alpha}{G_{13}} + \frac{Sin^2\alpha}{G_{23}}$$

$$c_{45} = (\frac{1}{G_{13}} - \frac{1}{G_{23}}) Cos\alpha Sin\alpha$$

$$c_{55} = \frac{Sin^2\alpha}{G_{13}} + \frac{Cos^2\alpha}{G_{23}}$$

Table 1: Effect of transverse shear and warping on the interacting load intensities and their distributions along the contact lines[a]

Component	Peak values of the interacting load intensity				Comments on the distribution, and figure number
	CLT[b] model Warping[c] neglected	CLT model Warping included	SDT[d] model Warping neglected	SDT Model Warping included	
λ_{xs} lb/in.	131. @ x/l = - 0.22	132. @ x/l = - 0.22	127. @ x/l = – 0.21	130. @ x/l = – 0.22	Antisymmetric; Non-zero over entire stringer length; Fig. 5
λ_{zs} lb/in.	767. @ x/l = - 0.02	613. @ x/l = 0.01	571. @ x/l = 0	571. @ x/l = 0	Symmetric; Small magnitudes except near origin; Fig. 6
λ_{xr} lb/in.	90.8 @ θ/Θ = 0	74.6 @ θ/Θ = 0	10.7 @ θ/Θ = 0	80.7 @ θ/Θ = 0	Symmetric; Small magnitudes except near origin; Fig. 7
$\lambda_{\theta r}$ lb/in.	63.2 @ $\theta/\Theta = \pm 0.04$	55.2 @ $\theta/\Theta = \pm 0.04$	49.0 @ $\theta/\Theta = \pm 0.21$	44.8 @ $\theta/\Theta = \pm 0.29$	Antisymmetric; Non-zero over entire ring length; Fig. 8
λ_{zr} lb/in.	- 886. @ θ/Θ = 0	- 883. @ θ/Θ = 0	- 854. @ θ/Θ = 0	- 852. @ θ/Θ = 0	Symmetric; Small values except near origin; Fig. 9
$\Lambda_{\theta r}$ in.-lb/in.	- 198. @ θ/Θ = 0	73.1 @ θ/Θ = 0	- 30.2 @ θ/Θ = 0	22.1 @ θ/Θ = 0	Symmetric; Nearly zero except near origin; Fig. 10
Λ_{zr} in.-lb/in.	3.21 @ $\theta/\Theta = \pm 0.03$	- 4.38 @ $\theta/\Theta = \pm 0.37$	- 3.95 @ $\theta/\Theta = \pm 0.37$	- 1.55 @ $\theta/\Theta = \pm 0.20$	Antisymmetric; Non-zero over entire stringer length; Fig. 11

a. Results for Fourier series truncated at 24 terms in the axial and circumferential directions.
b. CLT is classical lamination theory.
c. Out of plane warping of the ring's cross section due to torsion
d. First order transverse shear deformation theory

Table 2: Rotations about the circumferential axis at the stiffener intersection.

Description of the rotation of the structural component	Rotations in 10^{-5} radians			
	Classical theory		Transverse shear theory	
	No Warping	Warping	No Warping	Warping
Shell normal $\phi_x(0, 0)$	- 2.56	2.58	-1.06	2.65
Ring twist $\phi_{\theta r}(0)$	- 2.56	2.58	-2.67	3.64
Stringer normal $\phi_{\theta s}(0)$	- 2.56	2.58	-0.29	1.85

Table 3: Resultants at stiffener intersection.

Components of the resultant	Classical theory		Transverse shear deformation theory	
	Warping	No warping	Warping	No warping
C_θ from stringer, lb-in.	- 0.0921	- 1.1696	- 0.7797	- 0.2953
C_θ from ring, lb-in.	5.645	1.627	6.0192	1.363
C_θ total, lb-in.	5.5526	0.457	5.2396	1.0676
F_z, lb.	- 564.56	- 564.06	- 563.15	- 562.27

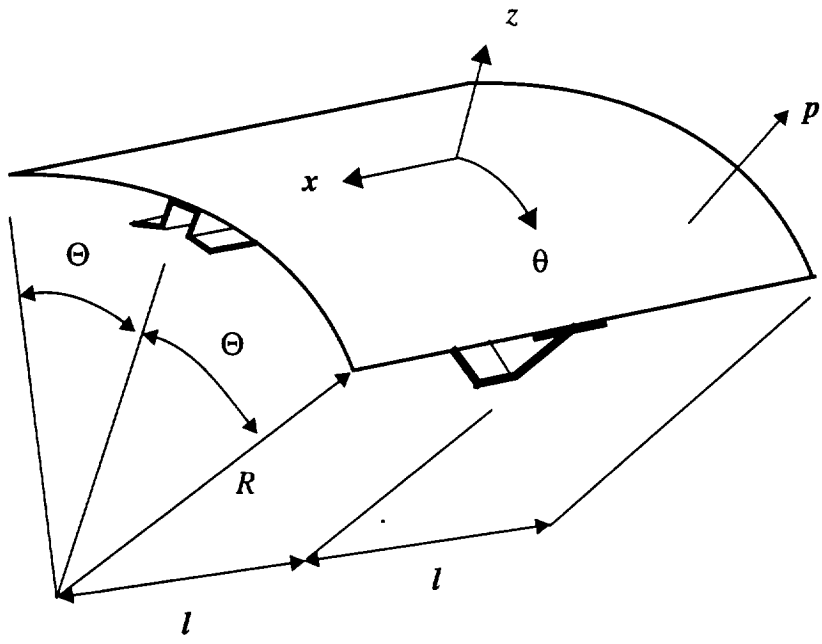

Fig. 1. Repeating unit of an orthogonally stiffened cylindrical shell.

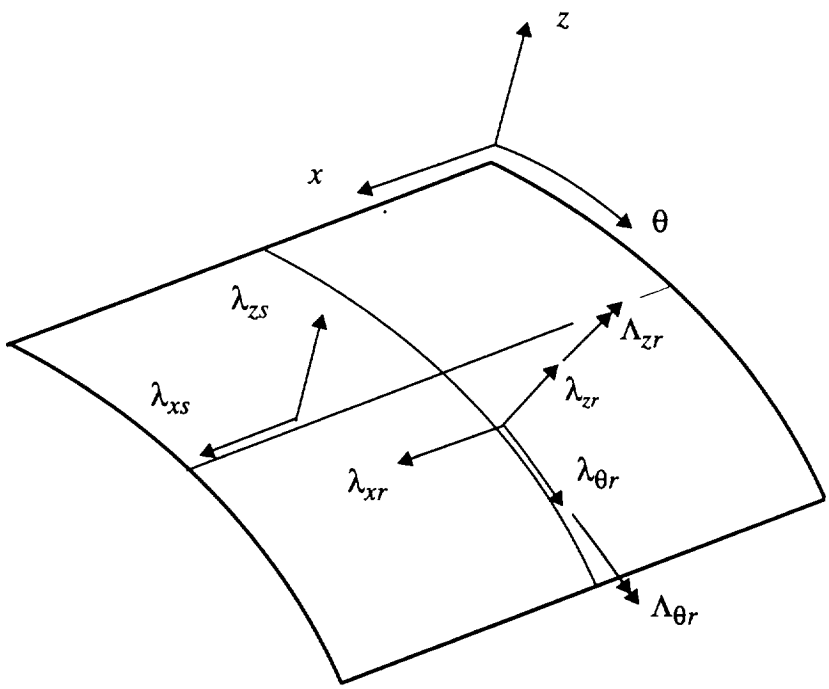

Fig. 2. Interacting line load intensities shown in the positive sense acting on the inside surface of the shell.

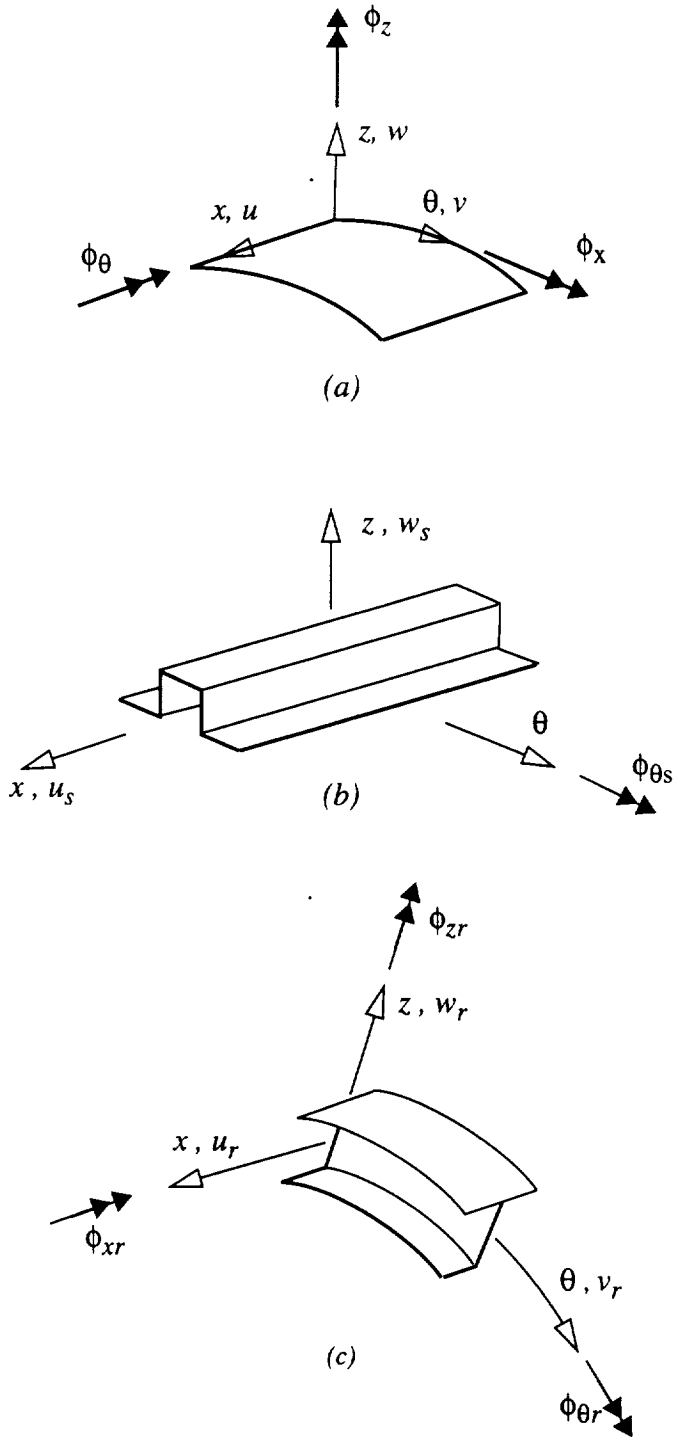

Fig. 3. Displacements and rotations for (a) shell, (b) stringer, and (c) ring

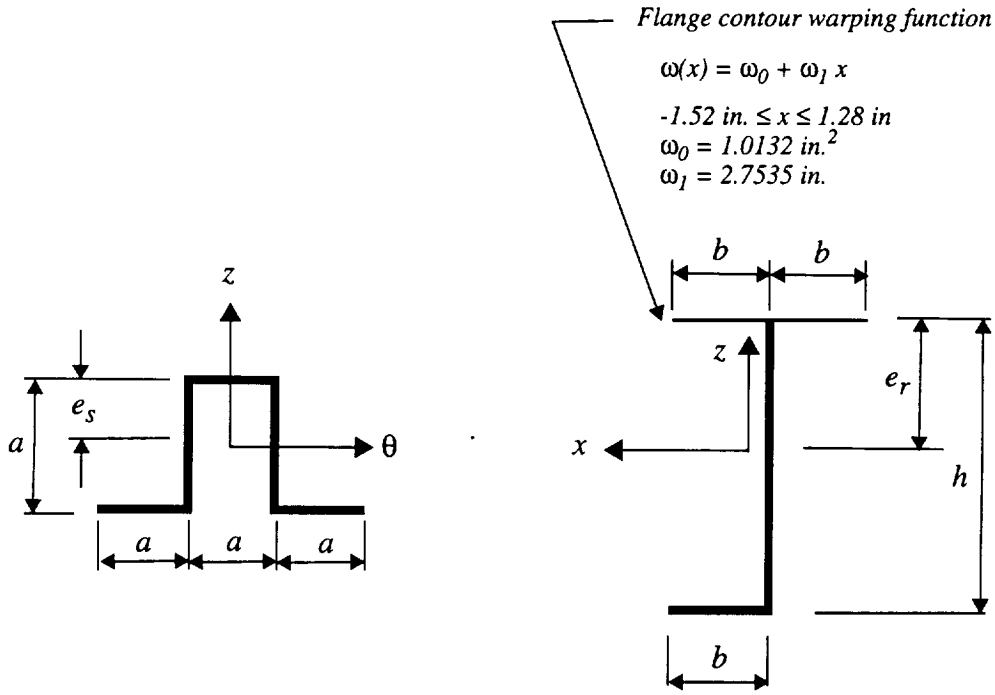

Stringer
$a = 1.4$ in.
$e_s = 0.8151$ in.

Ring
$h = 5.6$ in.
$b = 1.4$ in.
$e_r = 2.854$ in.

Fig. 4. Stiffener cross sections.

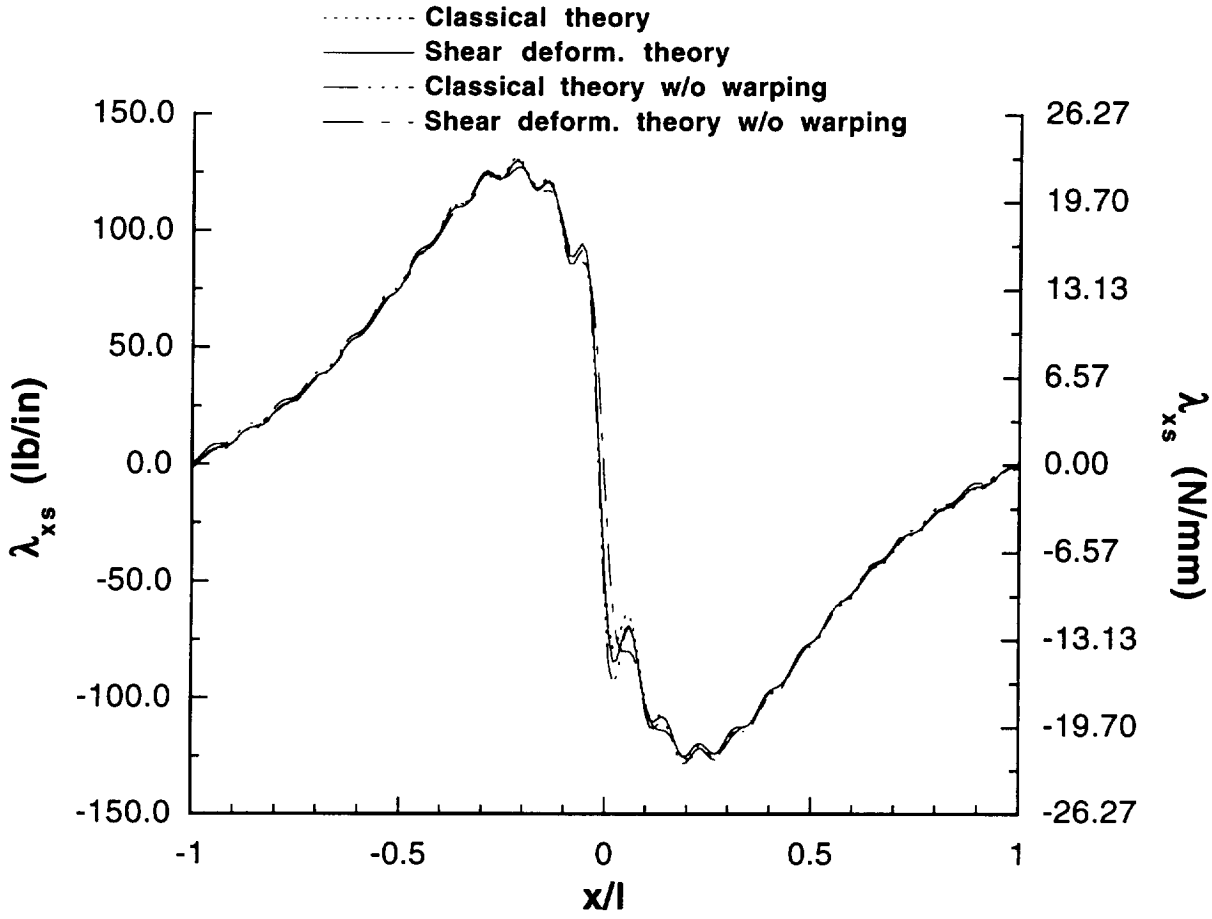

Fig. 5 Stringer-shell tangential force intensity in axial direction.

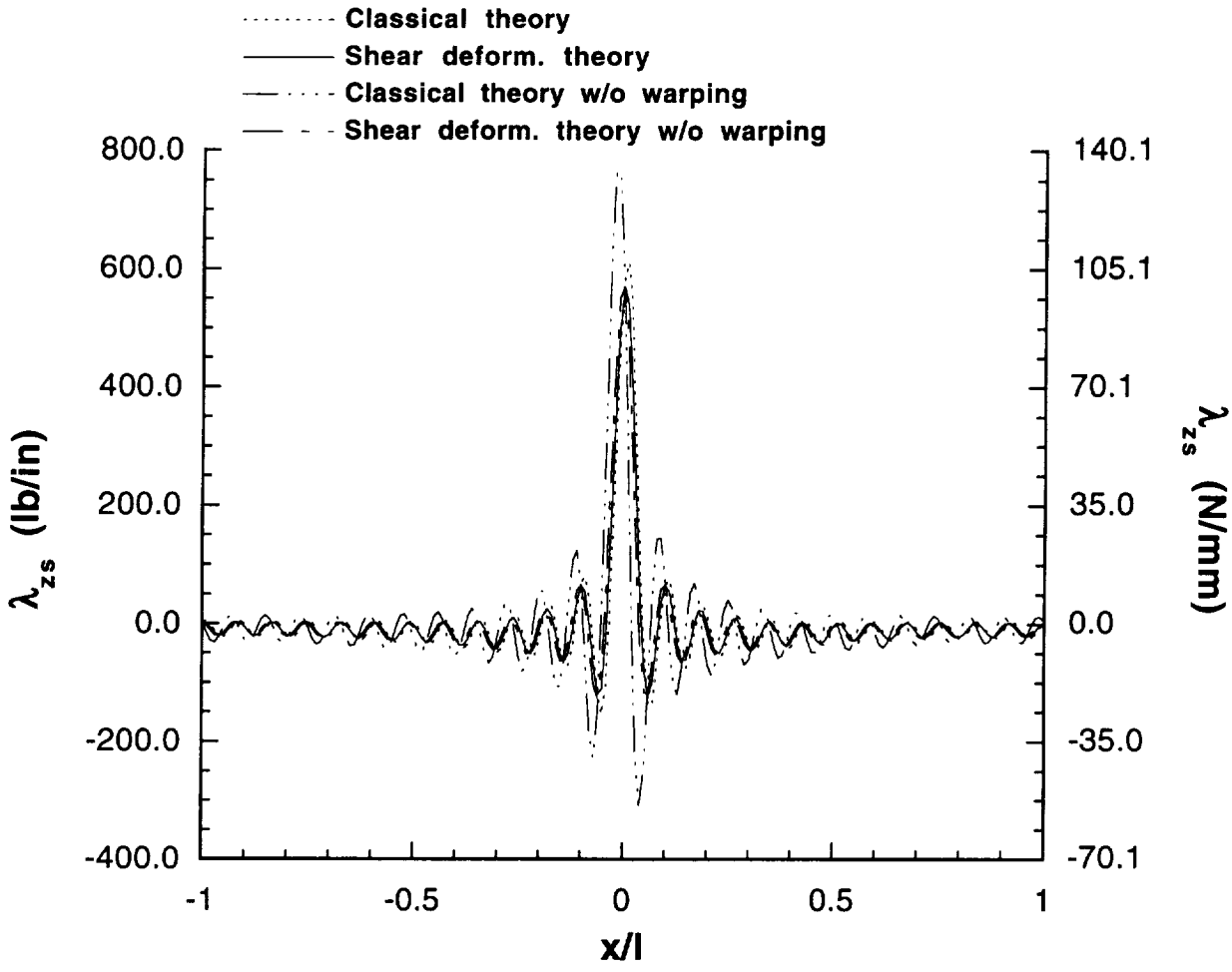

Fig. 6 Stringer-shell normal force intensity.

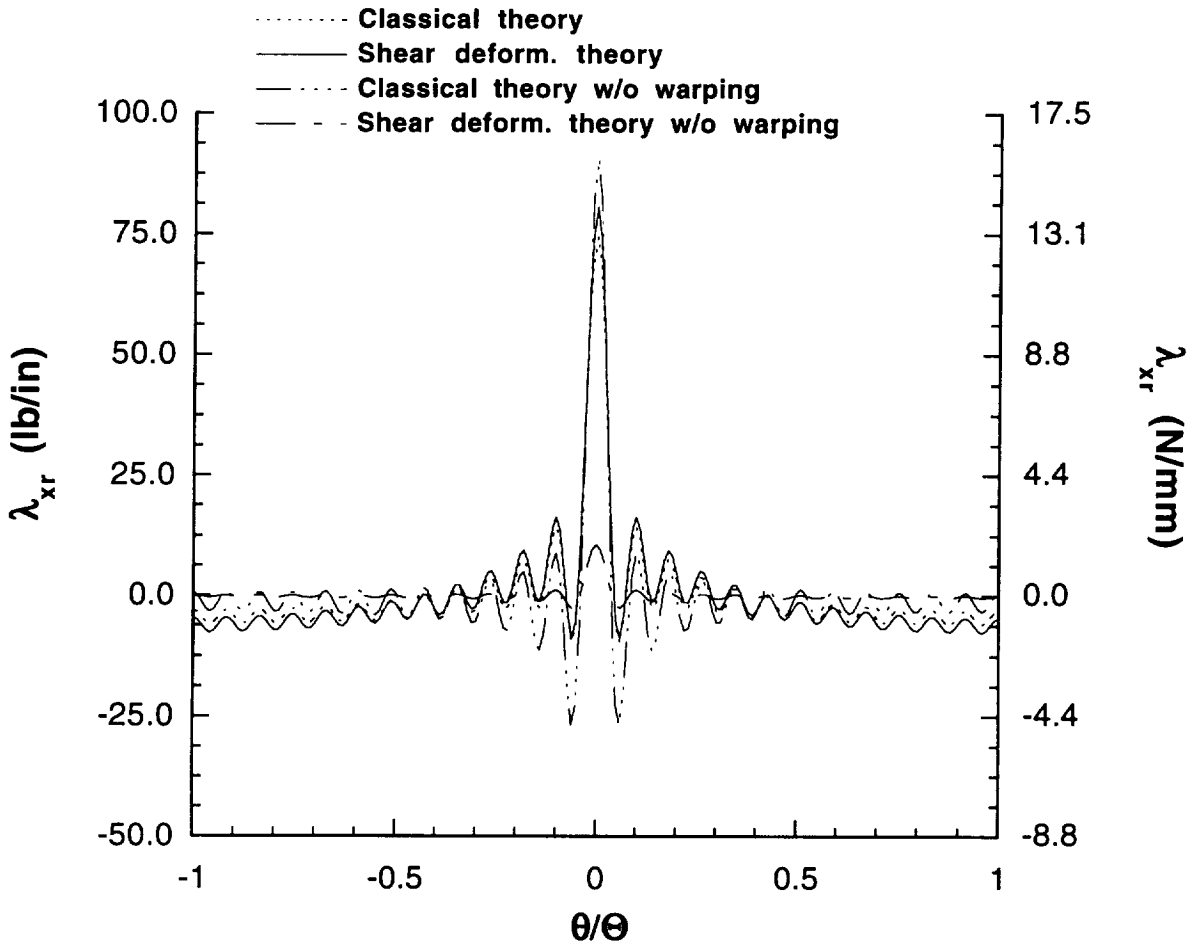

Fig. 7 Ring-shell tangential force intensity in axial direction.

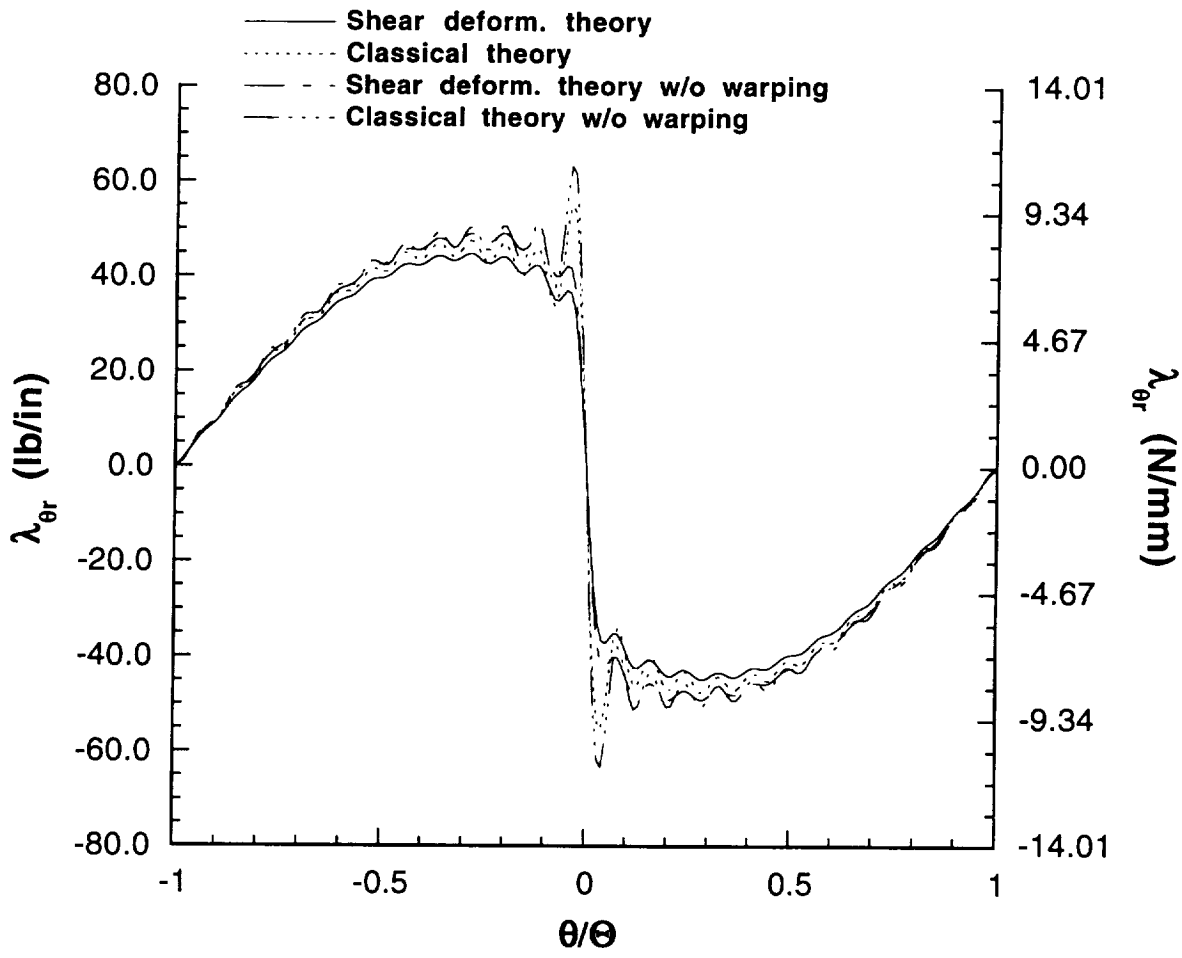

Fig. 8 Ring-shell tangential force intensity in circumferential direction.

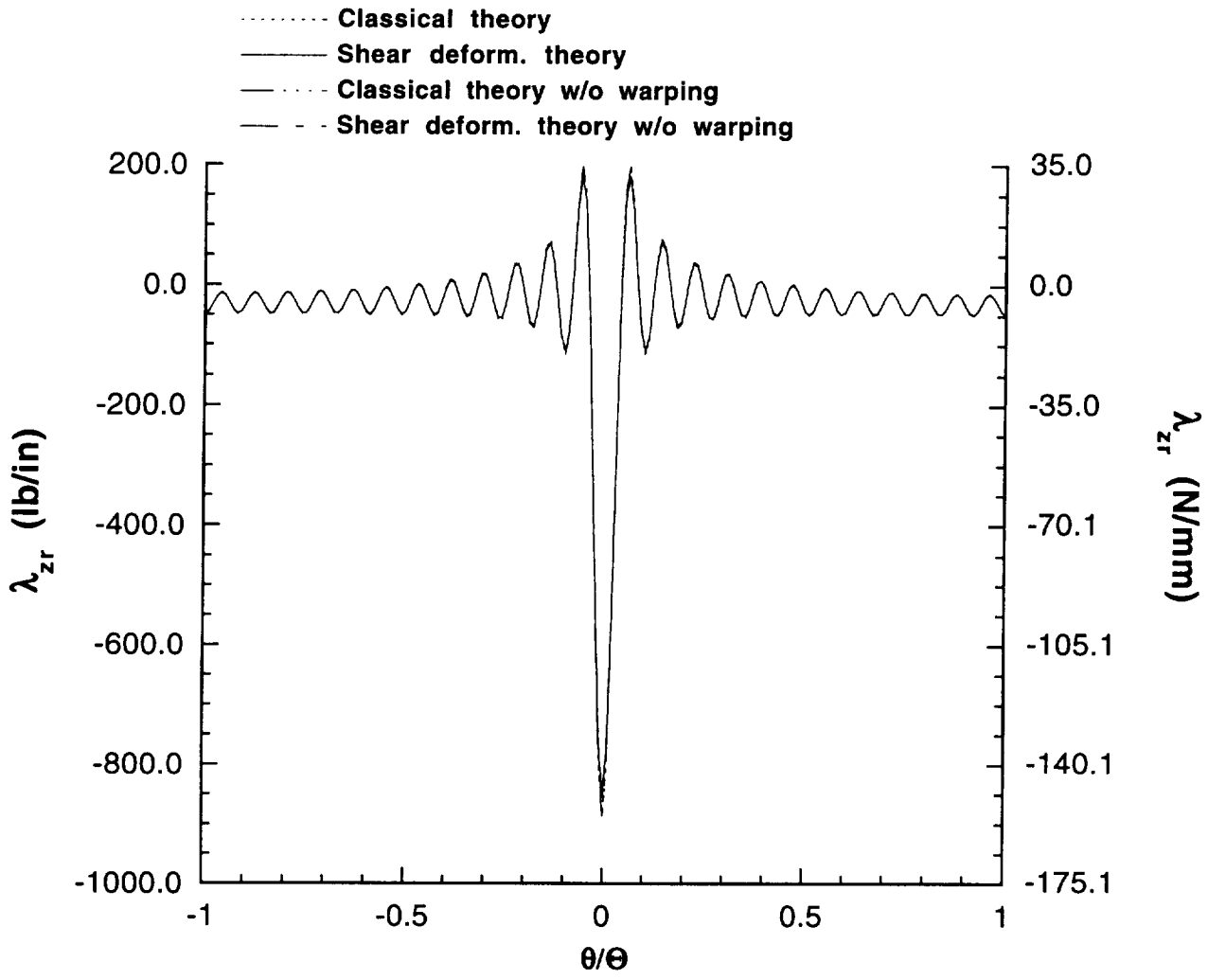

Fig. 9 Ring-shell normal force intensity.

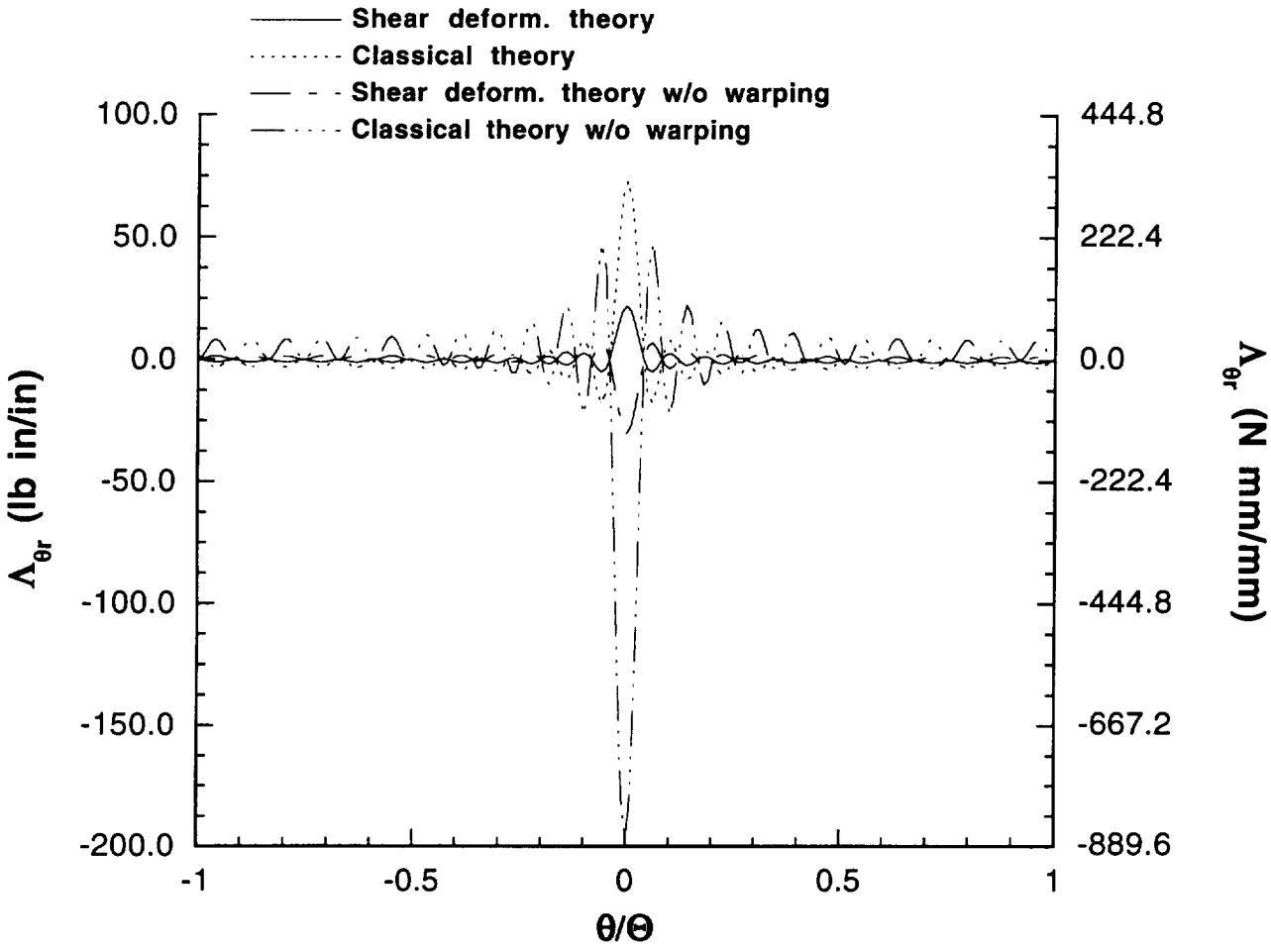

Fig. 10 Ring-shell tangential moment intensity in circumferential direction.

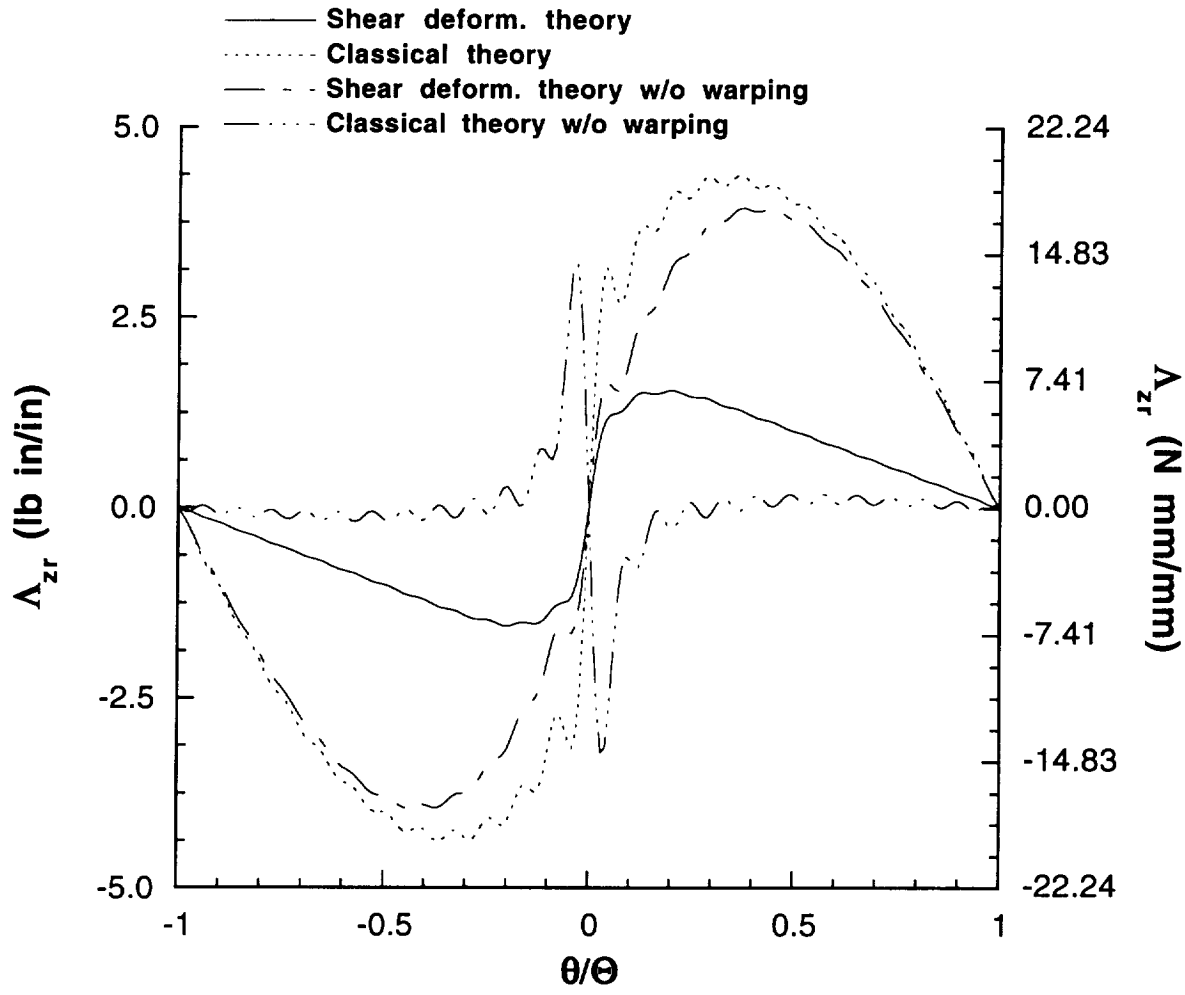

Fig. 11 Ring-shell normal moment intensity.

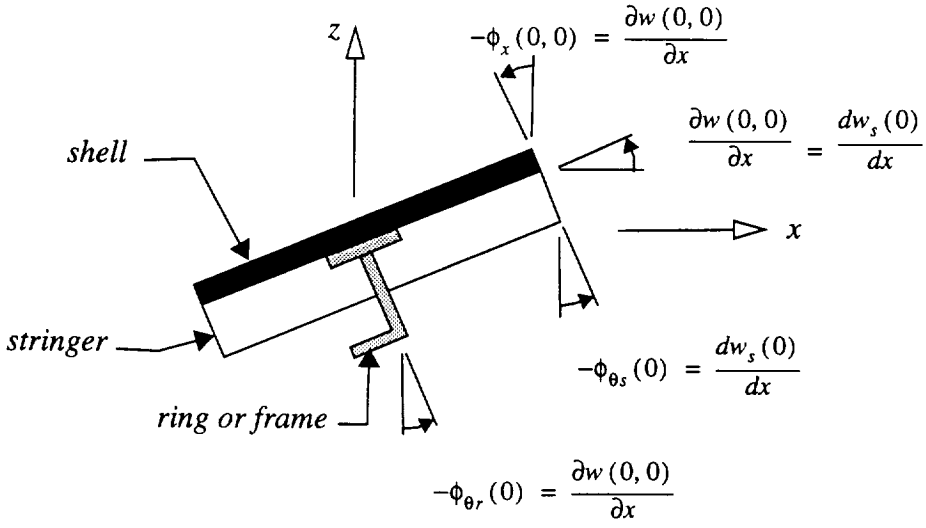

(a)

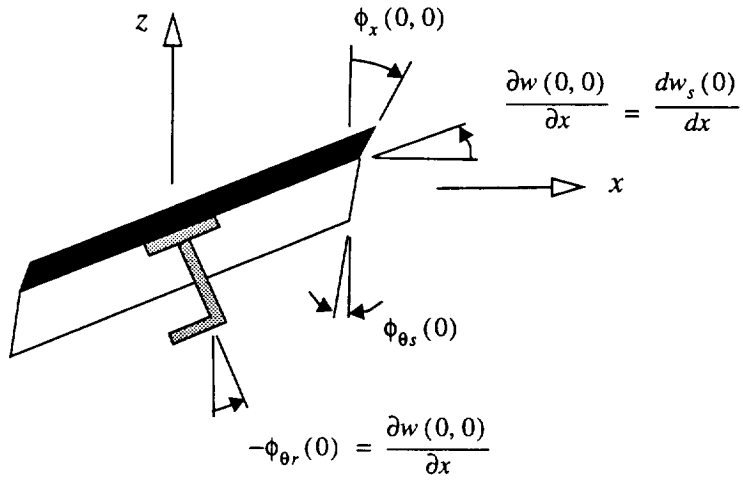

(b)

Fig. 12 Joint rotations for (a) the classical structural models, and (b) for transverse shear deformable models.

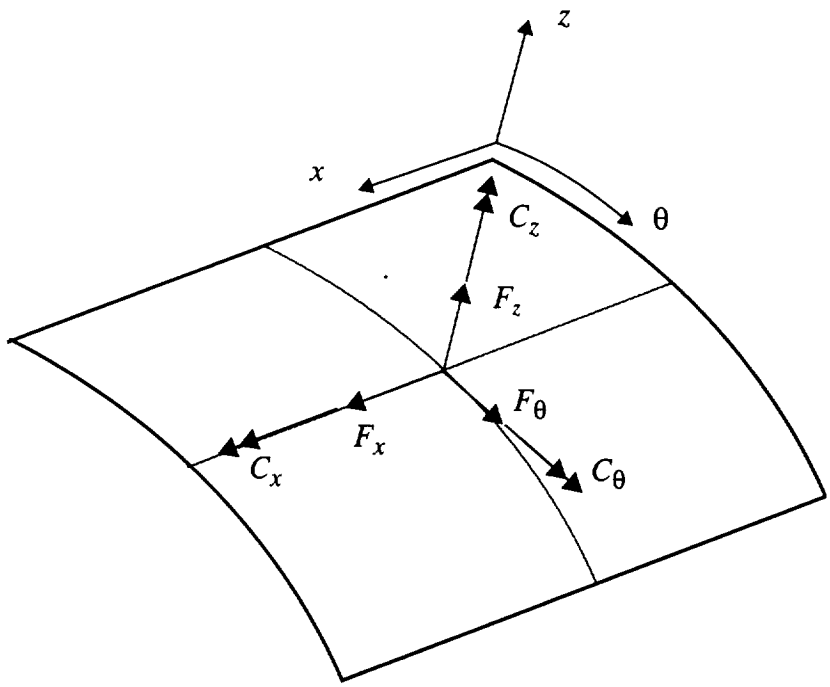

Fig. 13. Componets of the resultant of the interacting line load intensities acting on the inside wall of the shell at the origin.

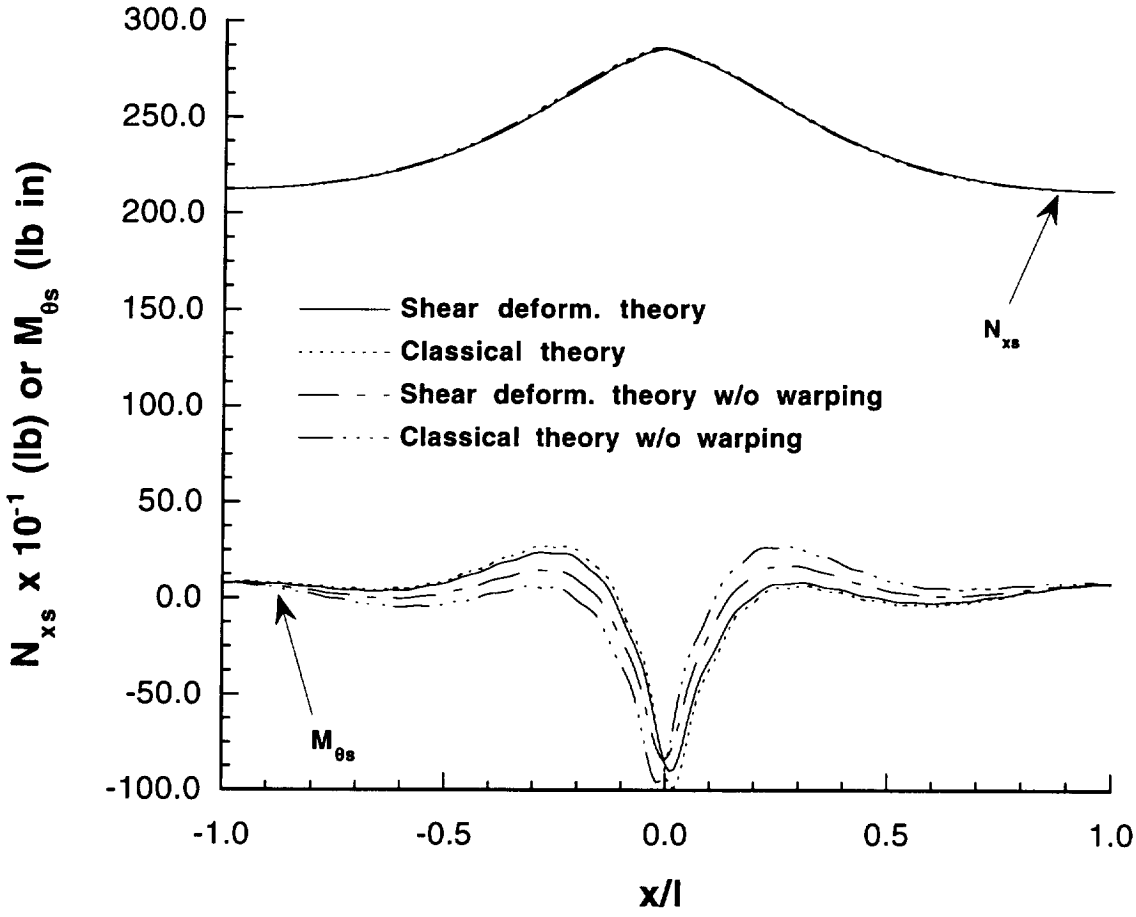

Fig. 14 Stringer axial force and bending moment distribution.

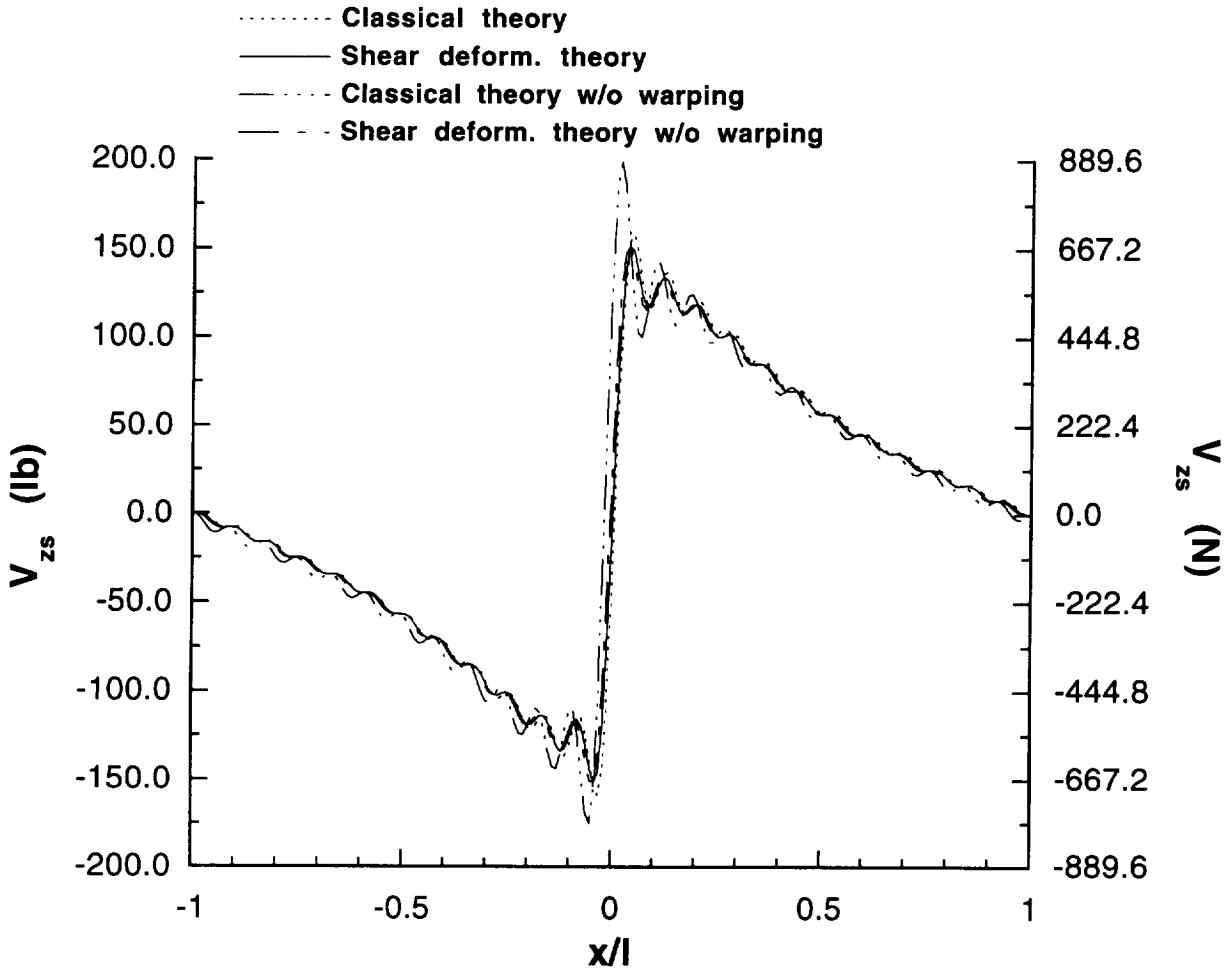

Fig. 15 Stringer transverse shear force distribution.

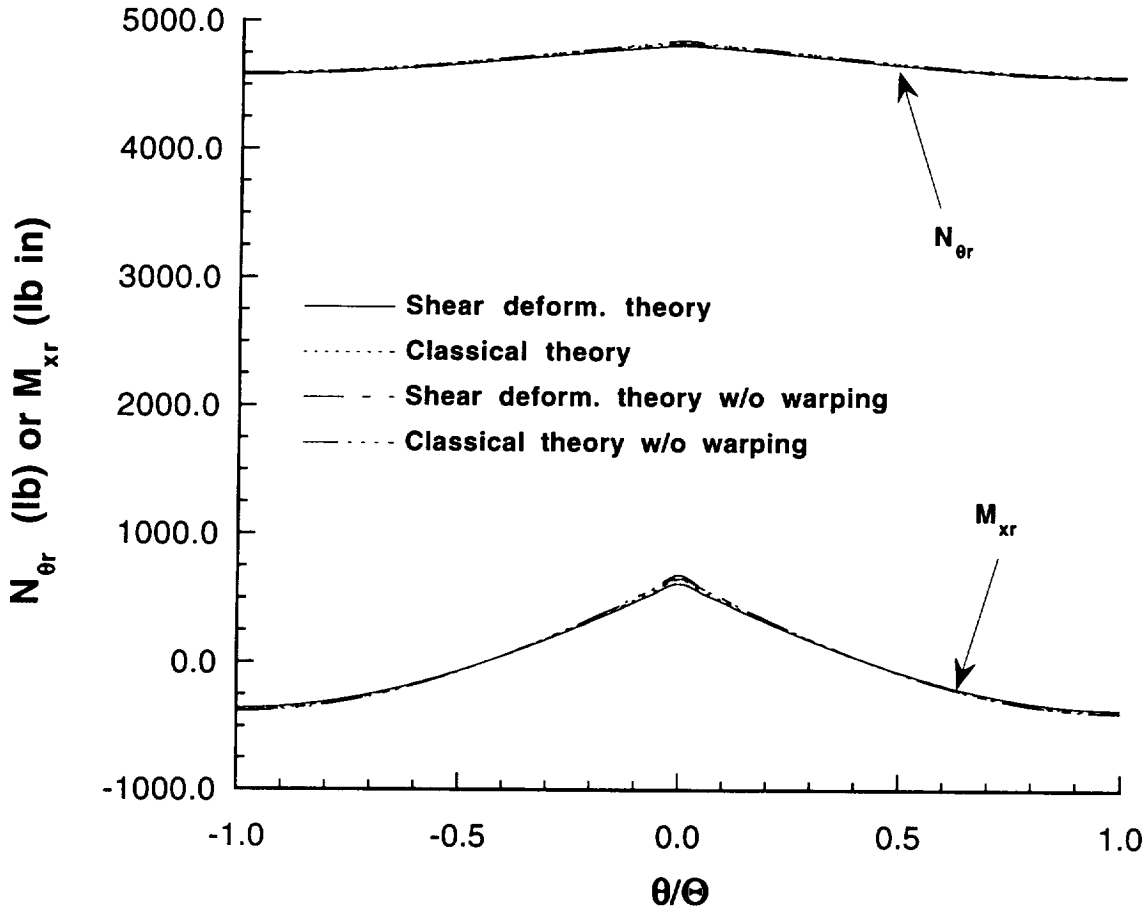

Fig. 16 Ring circumferential force and in-plane bending moment distribution.

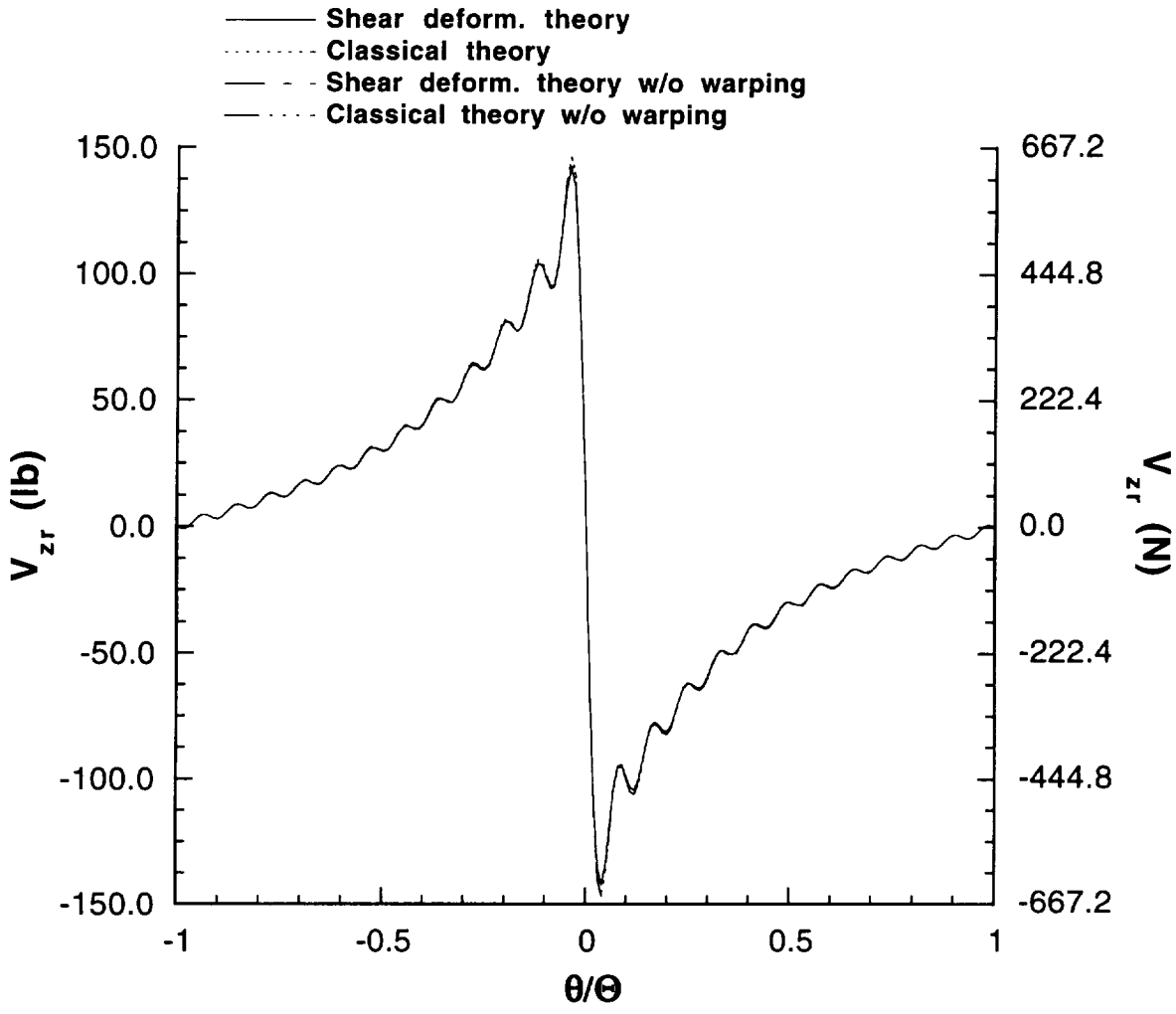

Fig. 17 Ring in-plane shear force distribution.

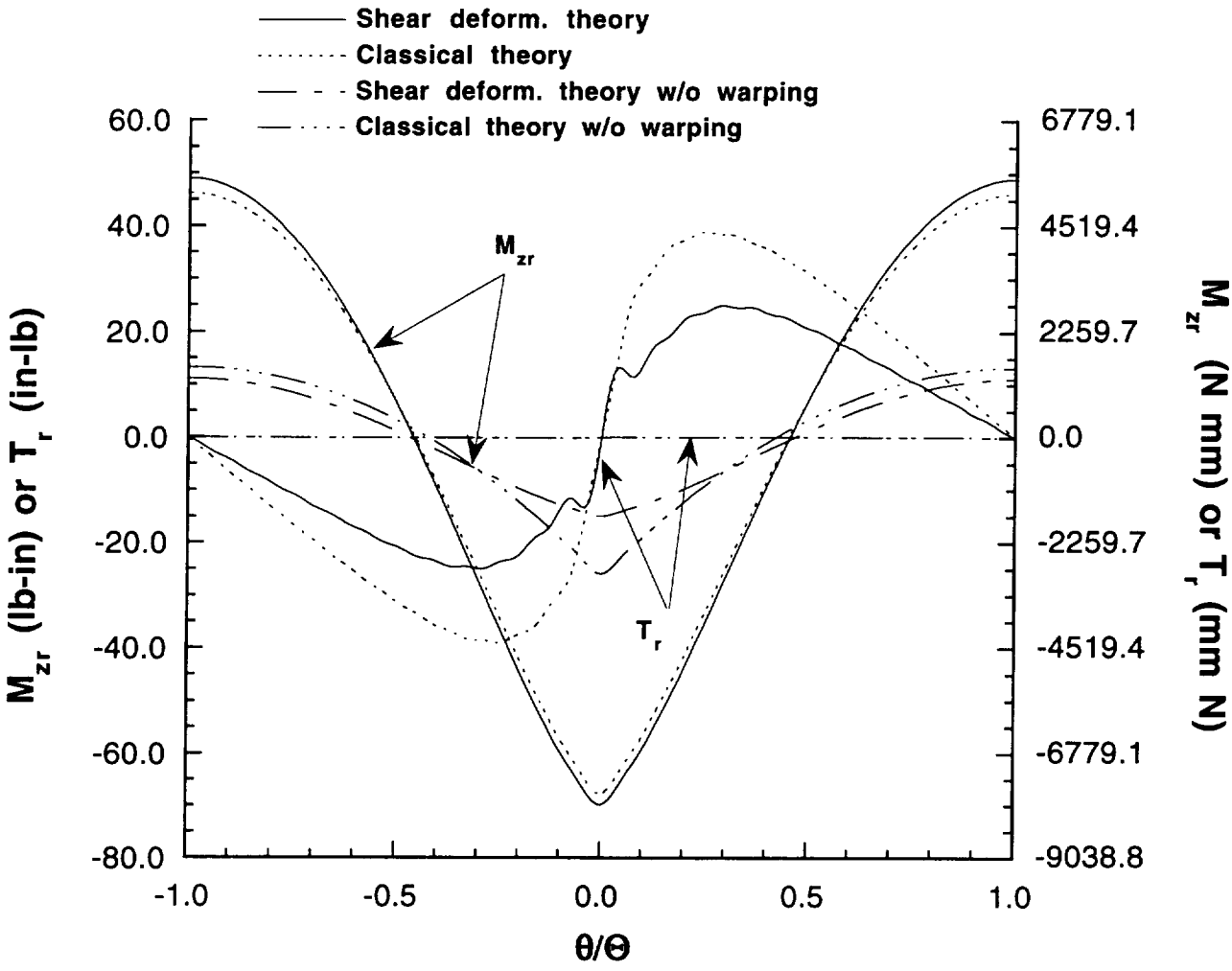

Fig. 18 Ring out-of-plane bending moment and torque distributions.

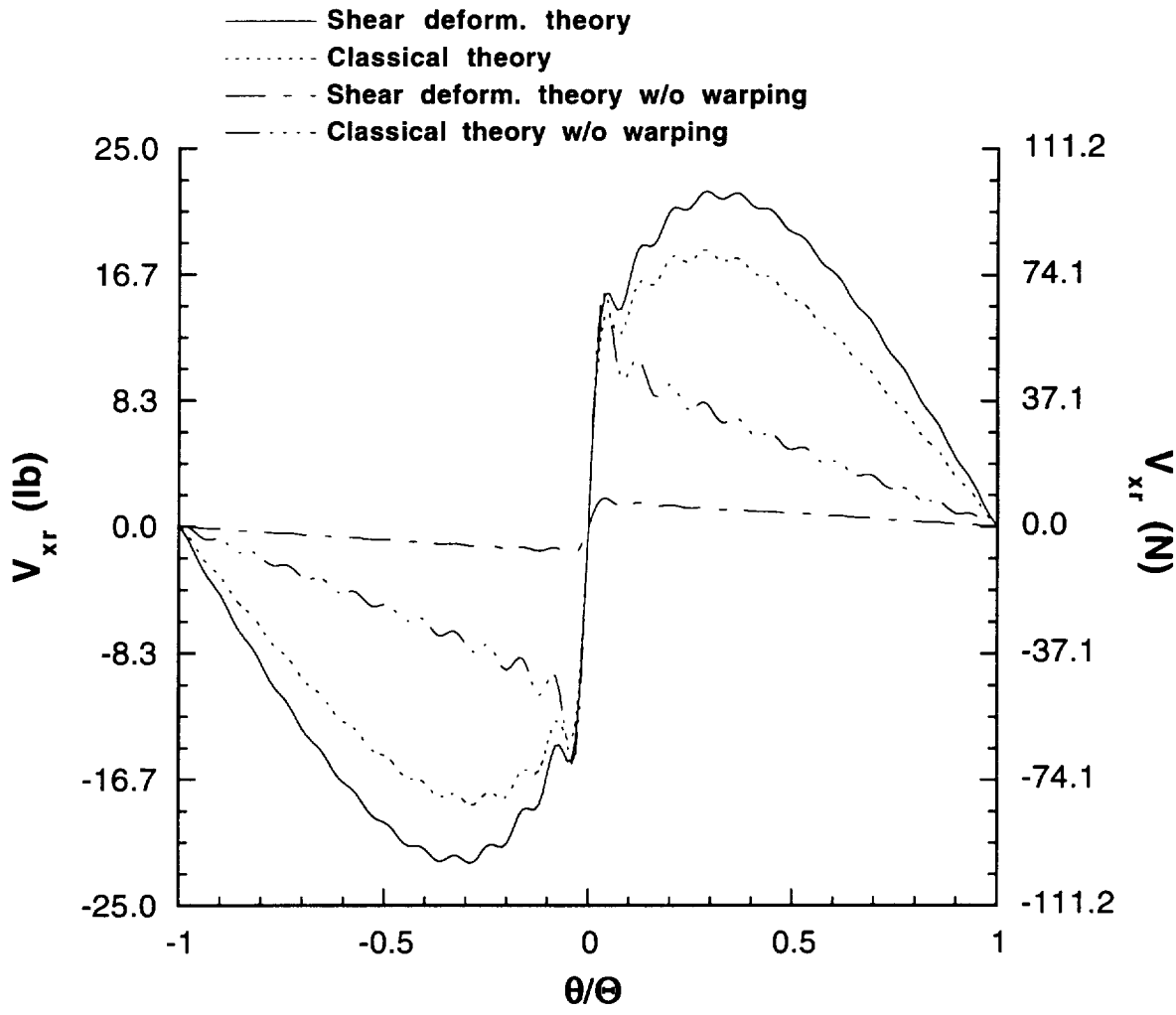

Fig. 19 Ring out-of-plane shear force distribution.